


Nicotinic Acetylcholine Receptors Expressed by Striatal Interneurons Inhibit Striatal Activity and Control Striatal-Dependent Behaviors

Alice Abbondanza,^{1,6} Irina Ribeiro Bas,¹ Martin Modrak,⁴ Martin Capek,^{3,5} Jessica Minich,¹ Alexandra Tyshkevich,¹ Shahed Naser,¹ Revan Rangotis,¹ Pavel Houdek,² Alena Sumova,² Sylvie Dumas,⁷  Veronique Bernard,⁶ and Helena Janickova¹

¹Laboratory of Neurochemistry, Institute of Physiology of the Czech Academy of Sciences, Prague, 14220, Czech Republic, ²Laboratory of Biological Rhythms, Institute of Physiology of the Czech Academy of Sciences, Prague, 14220, Czech Republic, ³Laboratory of Biomathematics, Institute of Physiology of the Czech Academy of Sciences, Prague, 14220, Czech Republic, ⁴Bioinformatics Core Facility, Institute of Microbiology of the Czech Academy of Sciences, Prague, 14220, Czech Republic, ⁵Light Microscopy Core Facility, Institute of Molecular Genetics of the Czech Academy of Sciences, Prague, 14220, Czech Republic, ⁶Neuroscience ParisSeine, Institut de Biologie Paris Seine, Institut National de la Santé et de la Recherche Médicale, Centre National de la Recherche Scientifique, Sorbonne Université, Paris, 75005, France, and ⁷Oramacell, Paris, 75006, France

Acetylcholine is an important modulator of striatal activity, and it is vital to controlling striatal-dependent behaviors, including motor and cognitive functions. Despite this significance, the mechanisms determining how acetylcholine impacts striatal signaling are still not fully understood. In particular, little is known about the role of nAChRs expressed by striatal interneurons. In the present study, we used FISH to determine which neuronal types express the most prevalent beta2 nicotinic subunit in the mouse striatum. Our data support a common view that nAChR expression is mostly restricted to striatal interneurons. Surprisingly though, cholinergic interneurons were identified as a population with the highest expression of beta2 nicotinic subunit. To investigate the functional significance of beta2-containing nAChRs in striatal interneurons, we deleted them by injecting the AAV-Cre vector into the striatum of *beta2-flox/flox* male mice. The deletion led to alterations in several behavioral domains, namely, to an increased anxiety-like behavior, decrease in sociability ratio, deficit in discrimination learning, and increased amphetamine-induced hyperlocomotion and c-Fos expression in mice with beta2 deletion. Further colocalization analysis showed that the increased c-Fos expression was present in both medium spiny neurons and presumed striatal interneurons. The present study concludes that, despite being relatively rare, beta2-containing nAChRs are primarily expressed in striatal neurons by cholinergic interneurons and play a significant role in behavior.

Key words: acetylcholine; behavior; Fos; interneurons; nAChRs; striatum

Received Aug. 10, 2021; revised Jan. 21, 2022; accepted Jan. 25, 2022.

Author contributions: V.B., A.A., A.S., S.D., and H.J. designed research; V.B., A.A., M.M., A.S., and H.J. wrote the paper; A.A., I.R.B., J.M., A.T., S.N., R.R., P.H., S.D., and H.J. performed research; A.A., I.R.B., M.M., M.C., J.M., P.H., S.D., and H.J. analyzed data; I.R.B., R.R., and S.D. edited the paper.

This work was supported by Grant Agency of the Czech Republic Grant 19-07983Y, Czech-Biolmaging Projects LM2015062 and LM2018129, and Mobility Project of the Czech Ministry of Education 8J21FR022. This work was further supported by Institut National de la Santé et de la Recherche Médicale, Center National de la Recherche Scientifique, Université Pierre et Marie Curie, Fédération pour la Recherche sur le Cerveau, and the French Ministry of Europe and Foreign Affairs (Partenariat Hubert Curien; Program Barrande). A.A. was supported by the Barrande Fellowship Program of the French Embassy in the Czech Republic and the Czech Ministry of Education, Youth and Sports. J.M. was supported by the Rise Worldwide program of the German Academic Exchange Service (DAAD). I.R.B. was supported by Erasmus+ program of the European Union. M.M. was

supported by ELIXIR CZ research infrastructure project (MEYS Grant LM2018131), including access to computing and storage facilities. We also acknowledge the Light Microscopy Core Facilities of IMG CAS and the Institute of Physiology CAS, Prague, Czech Republic, supported by MEYS CR (LM2018129, CZ.02.1.01/0.0/0.0/18_046/0016045) and RVO: 68378050-KAV-NPUI, for their support with the confocal imaging and image analysis herein. We thank Marie-Laure Niepon (Image platform at Institute de la Vision, Paris) for slide scanning; Dana Ungerova, Eva Suchanova, and Anna Smrckova for help with experiments; and Jan Jakubik, Vladimir Dolezal, Alena Randakova, and Ornela Kljatic for reading and valuable comments on the manuscript.

The authors declare no competing financial interests.

Correspondence should be addressed to Helena Janickova at helena.janickova@fgu.cas.cz or Veronique Bernard at veronique.bernard@inserm.fr.

<https://doi.org/10.1523/JNEUROSCI.1627-21.2022>

Copyright © 2022 the authors

Significance Statement

A large variety of nAChRs are expressed in the striatum, a brain region that is crucial in the control of behavior. The complexity of receptors with different functions is hindering our understanding of mechanisms through which striatal acetylcholine modulates behavior. We focused on the role of a small population of beta2-containing nAChRs. We identified neuronal types expressing these receptors and determined their impact in the control of explorative behavior, anxiety-like behavior, learning, and sensitivity to stimulants. Additional experiments showed that these alterations were associated with an overall increased activity of striatal neurons. Thus, the small population of nicotinic receptors represents an interesting target for a modulation of response to stimulant drugs and other striatal-based behavior.

Introduction

A growing body of evidence suggests that interneurons (INs) play a key role in controlling striatal functions despite the fact that they represent only a minority of striatal neurons (<5% in rodents) (Muñoz-Manchado et al., 2016; Lee et al., 2017; Rapanelli et al., 2017; Holly et al., 2019). Striatal INs are commonly divided into two main groups, cholinergic and GABAergic (CINs and GABAINs, respectively). In the past decade, electrophysiological studies indicated that, unlike the principal striatal neurons (commonly referred to as medium spiny neurons [MSNs]), certain types of INs express functional nAChRs. For instance, somatostatin-expressing, 5HT_{3A}-expressing, and neuropeptide Y-expressing (NPY⁺) GABAINs are activated by nicotine, and this activation leads to inhibition of MSN activity (English et al., 2011; Faust et al., 2016; Assous et al., 2017). These studies suggested that, although nAChRs are expressed by a relatively small number of striatal neurons, these receptors have the power to modulate striatal signaling and functions. Therefore, it has been hypothesized that nAChRs expressed by striatal INs play a significant role in the control of striatal-based behavior (e.g., supporting cognitive flexibility) (Faust et al., 2016; Assous, 2021), but direct evidence was missing. Recently, several novel types of GABAINs, each with distinct immunohistochemical and electrophysiological properties, have been described in the striatum (Muñoz-Manchado et al., 2016; Assous et al., 2018; Muñoz-Manchado et al., 2018). Including the classic groups of parvalbumin-, somatostatin- and calretinin-expressing neurons, striatal GABAINs now seem to be composed of at least seven distinct neuronal populations, and this number may grow. Although individual types of striatal INs express nAChRs in overall low levels and with varying subunit composition, beta2-containing nAChRs are relatively the most common type (Quik et al., 2009; Quik and Wonnacott, 2011). Until the emergence of single-cell RNA sequencing (scRNA-seq), detailed information on the expression of specific nicotinic subunits by individual types of striatal INs was lacking. A recent scRNA-seq study distinguishing between seven different types of striatal GABAINs suggested that each GABAIN population may express different types of nAChRs (Muñoz-Manchado et al., 2018). Specifically, TH-expressing GABAINs were shown to be distinguished by their expression of the alpha3 nicotinic subunit. Unlike the expression of the alpha3 subunit, the beta2 subunit was not specifically examined in the study by (Muñoz-Manchado et al., 2018). Thus, we used this previously published scRNA-seq data and reanalyzed it to assess and compare the expression of the beta2 subunit in different populations of striatal neurons (see Fig. 2*a,b*). Surprisingly, the reanalysis showed no difference in beta2 expression, not

only between the individual groups of GABAINs, but also between GABAINs and MSNs. Therefore, expression of beta2-containing nAChRs by striatal neurons requires further investigation.

In the present study, we used FISH with a probe targeting the beta2 nicotinic subunit to evaluate its expression in combination with markers for all major neuronal types present in the striatum. Unexpectedly, we found that the majority of beta2-containing nAChRs are expressed by striatal CINs and to lesser extent by other types of INs. Then, to evaluate a behavioral role of these receptors, we deleted beta2 nicotinic subunit specifically in striatal INs while keeping intact receptors expressed on dopaminergic and glutamatergic striatal terminals. A comprehensive behavioral analysis revealed that beta2 deletion in striatal INs leads to changes in several behavioral domains, including anxiety-like behavior, social and explorative behavior, discrimination learning, and sensitivity to amphetamine. Finally, our analysis of c-Fos expression documented that these behavioral alterations are accompanied by increased activation of striatal neurons, both MSNs and INs.

Materials and Methods

Animals

All experimental procedures complied with the directive of the European Community Council on the use of laboratory animals (2010/63/EU) and were approved by the respective local animal research committees. Mice were housed in a temperature and humidity-controlled room with a 12 h light/dark cycle (lights ON at 6:00 A.M. local time). Standard rodent chow and water were provided *ad libitum*. For the food-motivated T-maze task and instrumental task in the operant box mice were mildly food-restricted, and their weight was kept at 85%–90% of their free-food weight. For assessment of behavioral responses to temporal restriction of access to food, the pellets were removed from the cages 3 h after the lights on, and they were returned back 6 h later. The regimen continued for 10 d. The FISH experiments were performed in 3 C57BL/6J WT male mice. In the rest of the study, a total number of 80 *beta2-flox/flox* mice were used. The original breeding pairs of *beta2-flox/flox* mice were kindly provided by Prof. Michael Crair from Yale University; their generation and genotyping protocol was described in detail previously (Burbridge et al., 2014). The mice originally provided were homozygous on a mixed background, and we maintained them as such throughout the study (for 10 generations). After detecting behavioral differences between sexes in our pilot experiments, we decided to exclusively use male mice in our behavioral and biochemical experiments. Mice between the ages of 2 and 8 months were used throughout the study, and the maximum age difference within a single cohort was 40 d. After the stereotaxic surgery, some mice were separated and housed individually. To diminish any effect of the cage/litter, whenever possible, AAV-Cre injected and control animals were always included in one cage.

Experimental design and statistical analysis

Four independent cohorts of mice were injected into the dorsal striatum (DS) and used for behavioral experiments, and three of these cohorts

were used for *c-Fos* analysis. Cohorts 1&2 and Cohorts 3&4 always underwent the same behavioral tests. Selected tests were performed in all four cohorts and data pooled together. This resulted in some age differences between Cohorts 1&2 versus Cohorts 3&4 when tested in specific tasks. Data for split performance of mice in the different cohorts are shown in Figure 8*f–g*. Animals were pseudorandomly assigned to an experimental group (mice with the *beta2* deletion) and a control group so that each litter/cage included both groups if possible. Behavioral, immunofluorescence (IF), and qRT-PCR data were analyzed using GraphPad Prism versions 7 and 8 (GraphPad Software). We used two-tailed Student's *t* test for comparison of two experimental groups with the following exceptions where the data were not normally distributed: the number of dippings in the hole-board test was analyzed with a negative-binomial regression using the *glm.nb* function of the package MASS (Venables et al., 1994); the nest-building test was analyzed using a Bayesian zero-one-inflated β regression on the proportion of material used, via the *brms* package (Bürkner, 2017); the forced swim test, the examination time of the non-social object, and the sociability ratio in the social preference test were assessed with a γ regression using the “*glm*” function in R. The percentage of *c-Fos*-positive CINs was analyzed by generalized linear mixed model. Two-way ANOVA or repeated-measures two-way ANOVA followed by Sidak's or Tukey's *post hoc* tests were used to evaluate the effects of two variables. In cases where some values were missing (in tests of reversal learning where some mice were analyzed in the acquisition only since they failed to reach the acquisition criteria and could not be moved to the reversal phase), we used a mixed-effects analysis followed by post-tests. Significance was set at $p < 0.05$. Throughout the manuscript, we report data as mean \pm SEM and statistical analysis including *p* values and 95% CIs for the differences in means.

Reanalysis of *Chrn2* scRNA-seq data

To assess between-population differences in *Chrn2* expression, we used a Bayesian hierarchical GLM with negative binomial response and varying intercepts for both cell population group (glia, INs, MSNs) and the individual populations, using the *brms* R package (Bürkner, 2017). To account for differences in sequencing depth, we used the *estimateSizeFactors* function from the DESeq2 R package (Love et al., 2014). Plots were created with the *ggplot2* package (Wickham, 2016).

Code accessibility

The complete code to reproduce the analysis can be accessed at https://github.com/cas-bioinf/chrn2_striatum/blob/main/Chrn2_scRNA_reanalysis.Rmd.

Double-probe FISH

Adult mice (12.5 weeks) were killed by cervical dislocation. Brains were removed, rapidly frozen in cold isopentane (-30° – -35° C), and serially sectioned in 10 series on cryostat at 16 μ m thickness. Sections for each brain have been processed by ISH to allow systematic quantitative analysis throughout the whole striatum. Double-probe FISH was performed as previously reported (Dumas and Wallén-Mackenzie, 2019).

Probes. Double-probe FISH was performed using antisense riboprobes for the detection of the following mRNAs: *Chrn2*, NM_009602 sequence 597–1517; *Drd1*, NM_010076 sequence 1756–2707 and *Drd2* NM_010077 sequence 268–1187; *Chat*, NM_009891 sequence 526–1065; *Pvalb*: NM_013645 sequence 74–591; *Npy*, NM_023456 sequence 13–453; *Sst*, NM_009215 sequence 143–401; *Htr3a*, NM_013561 sequence 641–1552. Synthesis of digoxigenin (DIG) and fluorescein-labeled RNA probes were made by a transcriptional reaction with incorporation of digoxigenin or fluorescein labeled nucleotides (Sigma-Aldrich; Reference 11277073910 and 11685619910). Specificity of probes was verified using NCBI blast.

Procedure. Cryosections were air-dried, fixed in 4% PFA, and acetylated in 0.25% acetic anhydride/100 mM triethanolamine, pH 8, followed by washes in PBS. Sections were hybridized for 18 h at 65°C in 100 μ l of formamide-buffer containing 1 μ g/ml DIG-labeled riboprobe and 1 μ g/ml fluorescein-labeled riboprobe. Sections were washed at 65°C with SSC buffers of decreasing strength, and blocked with 20% FBS and 1% blocking solution. For revelation steps, DIG epitopes were detected with

HRP anti-DIG fab fragments at 1:2500 (Sigma-Aldrich; Reference 11207733910) and revealed using Cy3-tyramide at 1:100. Fluorescein epitopes were detected with HRP anti-fluorescein fab fragments at 1:5000 (Sigma-Aldrich; Reference 11426346910) and revealed using Cy2-tyramide at 1:250. Nuclear staining was performed with DAPI. All slides were scanned at 20 \times resolution using the NanoZoomer 2.0-HT (Hamamatsu Photonics). Laser intensity and time of acquisition were set separately for each riboprobe. Images were analyzed using the NDP.view2 software (Hamamatsu Photonics). ROIs were identified according to the Paxinos mouse brain atlas (Franklin and Paxinos, 2008). Positive cells refer to a staining in a cell body clearly above background and surrounding a DAPI-stained nucleus. Colocalization was determined by the presence of the signals for both probes in the soma of the same cell. A manual counting was performed. The entire ROI was evaluated. A mean of 700, 1200, 520, and 830 Chat, Npy, Pvalb, and Sst neurons, respectively, was analyzed per brain, on adjacent sections at 6 levels of rostro-caudal axis. For illustration purposes, the NanoZoomer images were exported in TIFF format using NDP viewer. Images were corrected for contrast, cropped on Photoshop 2021 (Adobe Systems), and assembled on Illustrator 2021 (Adobe Systems).

Stereotaxic surgeries

Beta2-flox/flox mice were injected with the AAV5-eGFP or AAV5-Cre-GFP viral vectors (viral titer 4.5×10^{12} vg/ml; UNC Vector Core) at 2 months of age. After mice were anesthetized by a mixture of ketamine (87 mg/kg) and xylazine (13 mg/kg; both Vetoquinol), they were placed in the stereotaxic frame (Stoelting). Animals were injected with a total volume of 1 μ l per hemisphere using four injections in total with the following coordinates: AP 1.5; ML 1.4; DV -3.0 and AP 1.3; ML ± 1.6 ; DV -3.3 . A microinjection pump (MICRO2T-UMP3-NL2010, World Precision Instruments) was used for the infusions with a speed rate of 50 nl/min. For the behavioral experiments, we injected 36 and 29 AAV5-Cre and AAV5-GFP mice, respectively. Viral expression was verified in all animals by IF after completion of behavioral tests, and 4 AAV5-Cre-injected animals were excluded from the study based on either insufficient or excessive expression of the virus. We considered expression insufficient when viral expression was completely absent from one or both hemispheres and excessive when it was significantly leaking into the hippocampus, thalamus, and/or cortex. IF analysis showed that the virus was leaking into striatal neighboring structures. However, the leaking was mostly unilateral, varied between mice, and did not systematically occur in a specific structure. The only exception was the lateral septum, which showed bilateral viral expression in two-thirds of the AAV5-Cre-injected animals (23 of 32). Except for the lateral septum, any other structure with bilateral viral expression always occurred in less than half of the injected animals (see Fig. 5*d*). To understand how the variability in AAV injections could affect the investigated behavior, we also used a subset of animals to analyze selected behavioral data in correlation to the extent of the AAV expression in the DS. However, none of the analyzed behavioral parameters reached a significant correlation with the AAV expression (see Fig. 8*a–e*).

PCR and qRT-PCR

To obtain samples for the PCR, mice were killed by decapitation, brains were quickly removed, and individual brain regions were dissected on ice, frozen on dry ice, and stored at -80° C until use. DNA for the endpoint PCR and RNA for the qRT-PCR from nonstriatal regions were isolated using TriPure Isolation Reagent (Roche) and treated with DNase (Sigma). RNA for the qRT-PCR from the striatum-expressing AAV virus was prepared from punches taken specifically in the AAV-expressing area and isolated by RNeasy Micro Kit (QIAGEN). The endpoint PCR was used to confirm the deletion of exon 5 of the *Chrn2* gene induced by the AAV-Cre injection into the DS of *beta2-flox/flox* mice. The primers used were 198#, 199#, and Bot2-09 as described by Burbidge et al. (2014). The endpoint PCR was performed with Taq DNA Polymerase (GeneDireX) according to the manufacturer's instructions, and DNA fragments were visualized on an agarose gel. For the qRT-PCR, the reverse transcription of the RNA samples was performed with LunaScript RT SuperMix (New England Biolabs) and the qPCR with

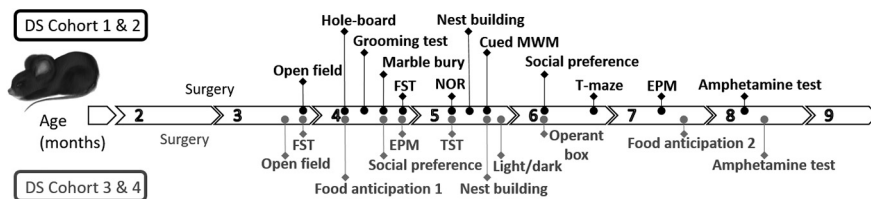


Figure 1. Behavioral tests performed in individual cohorts of mice. The order of tests in each cohort and the approximate age of tested animals are shown. We indicate each month of age with an arrow; each arrow can host 4 dots representing the 4 weeks of the month. On this timeline, we are showing the order of the behavioral tasks in the two different cohorts. The maximum age gap between the youngest and oldest animals in the cohorts is 6 weeks.

LCC 480 SYBR Green Master at LCC 480 instrument (Roche) according to the manufacturers' instructions. Primers used in qRT-PCR were targeted against exon 5 of the *Chrn2* gene: forward 5'-TGGCCATCC TGGTCTTCTAC-3' and reverse 5'-CGCCAGCAGCACAGAAATAC-3'. Beta-actin gene expression was used for normalization of the data using primers reported by Frahm et al. (2011). The relative quantification of gene expression was done using the $2^{-\Delta\Delta CT}$ method.

RNAscope analysis of the *Chrn2* expression

Mice were killed by decapitation. The brain was removed from the skull and immediately frozen in isopentane precooled in dry ice ($\leq 35^\circ\text{C}$), embedded in OCT medium, and stored at -80°C for up to 3 months. On the day of slicing, the OCT block was placed in the precooled cryostat (Leica CM 3000) at -20°C for 1 h before being sectioned sagittally at $16\ \mu\text{m}$. Sections that contained both the DS and substantia nigra pars compacta (SNc) were selected for the *Chrn2* RNA visualization. For visualization, we used the RNAscope kit (ACDBio) and a custom-made probe for exon 5 of the *Chrn2* RNA following the manufacturer's instructions for fresh-frozen tissue. Briefly, brain sections were fixed in 4% PFA for 15 min and dehydrated in increasing concentrations of ethanol (50%, 70%, $2 \times 100\%$) for 5 min each. After 30 min of incubation with Protease IV (ACDBio), the slices were hybridized with the target probes (*Chrn2*, positive and negative controls) for 2 h in the humidified incubator at 40°C . Several washes and incubations at 40°C with the amplification reagents (Amp-1, Amp-2, Amp-3, and Amp-4) followed, as per the manufacturer's instructions. Finally, the samples were stained with DAPI (ACDBio) for 30 s and mounted with Prolong Gold antifade reagent (Thermo Fisher Scientific). The *Chrn2* RNA was detected with a Leica SP8 WLL MP confocal microscope with HC PL APO $63\times/1.40\text{NA}$ objective. For each animal, three confocal images of the DS and three of the SNc were analyzed by Fiji's manual multi-counting function throughout the z stacks ($3\ \mu\text{m}$ steps, 7 pictures). Five cells per picture were randomly selected, and the total number of puncta in 5 cells was scored and reported.

ELISA

Concentration of striatal DA was measured using DA ELISA kit (ImmuSmol) according to the manufacturer's instructions. Dissected striata from both hemispheres were pooled and homogenized in $400\ \mu\text{l}$ of 40 mM Tris, 1 mM EDTA, and 10 mM HCl. For the ELISA procedure, $10\ \mu\text{l}$ of $100\times$ diluted original homogenate was used. Absorbance was measured by spectrophotometer VICTOR Plate Reader (PerkinElmer) at a wavelength of 450 nm. The measurement was done in two separate batches. To control for differences between the two measurements, we expressed the results as a percentage of controls.

Behavioral testing

All behavioral testing except the light/dark transition test was performed during the light phase (8:00 A.M. to 6:00 P.M.). Mice between the ages of 3 and 8 months were behaviorally tested with testing being initiated 1 month after stereotaxic surgery. The order of behavioral tests performed in individual cohorts was as follows (Fig. 1): Cohorts 1 and 2: locomotor activity in the open field \rightarrow hole-board test \rightarrow grooming test \rightarrow marble burying test \rightarrow forced swimming test (FST) \rightarrow novel object recognition (NOR) \rightarrow nest

building \rightarrow cued Morris water maze (cued MWM) \rightarrow social preference task \rightarrow T-maze task \rightarrow elevated plus maze (EPM) \rightarrow amphetamine-induced hyperlocomotion. Cohorts 3 and 4: open field \rightarrow FST \rightarrow first evaluation of food-anticipatory activity \rightarrow social preference task \rightarrow EPM \rightarrow tail suspension test (TST) \rightarrow nest building \rightarrow light/dark transition \rightarrow instrumental learning with reversal in the operant box \rightarrow second evaluation of food-anticipatory activity \rightarrow amphetamine-induced hyperlocomotion. Before each behavioral testing, mice were habituated to the testing room for at least 30 min.

Nest building. Nest building behavior was evaluated as described by Deacon (2006). Mice were first individually housed in new clean home cages. After 5 h of habituation in the home cage and at least 3 h before the onset of the dark phase, 2.8–3 g of cellulose nestlet material was distributed in each cage. The nest building activity was then evaluated using a scoring scale from 0 (untouched material) to 4 (complete, round, 3D nest), at times 10, 30, 60, and 180 min after material introduction. After 24 h, a last evaluation was recorded and the total amount of untorn material was weighed.

Locomotion in the open field. Mice were placed in the middle of a square Plexiglas arena $40 \times 40\ \text{cm}$, and their locomotor activity was recorded using a camera for 30 min in 2 consecutive days. The total distance traveled, together with the time spent in the center and edges of the box, was analyzed by ToxTrac software (Rodríguez et al., 2018). To test the acute effect of amphetamine, mice were habituated to the arena for 30 min, then injected intraperitoneally with either saline or amphetamine (Sigma) dissolved in saline (2 mg/kg) (Yates et al., 2007). After the injection, mice were returned to the arena and recorded for an additional 90 min. Immediately after the test, mice were anesthetized and transcardially perfused for c-Fos analysis.

EPM. We followed the protocol by Walf and Frye (2007). Mice were placed in the center of a cross formed by two open and two closed arms. Using a camera placed above the maze, any movements were recorded for 5 min. Based on the recordings, the time spent in each arm and number of entries were manually evaluated.

Light/dark transition. The light/dark transition task was used for assessing anxiety-like behavior (Crawley and Goodwin, 1980). Half of a Plexiglas $40 \times 40\ \text{cm}$ open field arena was enclosed in a black cardboard envelope and divided into two halves, light and dark, using a black partition. The black insert had a small opening in the front to allow the mouse to freely move between the light and the dark half of the arena. The test was done during the dark phase of the light cycle (active phase) in a bright room. Mice were placed in the center of the open part of the arena and allowed to freely explore both parts. The session was recorded and time spent in each part of the arena during the 10 min session was manually scored.

FST. The FST for assessment of depressive-like behavior was performed as described by Martyn et al. (2012). A 2 L beaker was filled with 1.8 L of tap water the temperature of which was maintained at 25°C – 27°C throughout the experiment. The water was changed every 3 or 4 animals. For testing, mice were gently placed into the beaker and recorded for 6 min. The time spent struggling for escape versus the time spent immobile was scored by an experimenter. Only 5 min of the test was scored as the first minute was not evaluated.

Evaluation of food anticipation. To determine the effect of the deletion on the food anticipation, the locomotor activity was monitored for 20 d. During the monitoring, the mice were maintained individually in cages equipped with infrared movement detectors attached above the cage in the center, which allowed for the detection of locomotor activity across the entire cage. The monitoring started under the standard *ad libitum* conditions for 10 d, and were followed by monitoring under the regimen during which the food access was restricted to only 6 h centered to the middle of the light phase of the light/dark cycle (Polidarová et al., 2013). A circadian activity monitoring system (H.M. Cooper, Institut

National de la Santé et de la Recherche Médicale) was used to measure activity at 1 min intervals. The resulting data were analyzed using the ClockLab toolbox (Actimetric). Double-plotted actograms were generated for visualization of data.

Social preference task. We assessed the sociability of our mice using a three-chamber Plexiglas apparatus (L × W × H, 90 × 23 × 23 cm) (Nadler et al., 2004). The two lateral compartments of the apparatus contained a wire mesh pen cup, and the middle compartment was empty. After 5 min of habituation in the apparatus, a novel juvenile (4–7 weeks old) male mouse was placed into one of the pen cups while the other remained empty. The tested animal was free to explore the compartments for an additional 10 min, and its behavior was recorded by a camera. The total time spent in each of the three compartments and the time spent interacting with the occupied and the unoccupied pen cup were evaluated manually by a blinded experimenter.

NOR. The procedure for testing memory was adapted from Zhang et al. (2012). On day 1, mice were habituated for 20 min in a clean empty home cage. The next day, mice were placed in the same cage for 10 min, and they were presented with two identical objects (small plastic black and white striped cups). After 1 h spent in their home cage, mice were placed back into the testing cage for 5 min where one of the cups was replaced with a similar but novel object (a small round plastic toy with a black stripe). Both the training and test sessions were recorded, and the time spent exploring each individual object was manually scored by a blinded observer. Based on the scores, the recognition index was expressed in percentage as Recognition index = time exploring novel object / (time exploring novel object + time exploring familiar object) × 100. A lack of innate bias for one of the two different objects was assessed by a pilot study.

Cued MWM. The cued version of the MWM was performed as described by Rossato et al. (2006), with the platform at water level, visible, and with a black and white striped flag as a cue. Mice were tested over 2 d with a novel platform and starting location each time. On day 1, the training consisted of 8 consecutive trials with a maximum duration of 60 s interleaved with a 60 s intertrial interval. After 24 h, mice were probed for their retention in 2 trials, starting from positions that were not used during the training. Latency to reach the platform and the distance traveled by the animal were recorded with a Tracker software (Biosignal Group) and analyzed by CM Manager version 0.4.0 (open source by Stepan Bahnik, available at: https://github.com/bahniks/CM_Manager_0_4_0).

Grooming test. Spontaneous and induced grooming was assessed by the grooming test. The test was performed as described by Wang et al. (2016). Before testing, mice were habituated to a novel empty cage for 5 min. After habituation, mice were recorded for 5 min (pre-spray phase), then removed from the cage and slightly misted with water from a spray bottle before being returned to the test cage. Recording continued for an additional 10 min (post-spray phase). Grooming events (number of events and their duration) were scored by a blinded experimenter.

Marble burying test. A compulsive-like behavior was tested using the marble burying test (Angoa-Pérez et al., 2013). Twenty glass marbles were positioned evenly on the surface of a 5-cm-high layer of clean bedding in a standard holding cage. Mice were recorded for 15 min, and the number of marbles buried was evaluated by a blinded experimenter. The marble was considered buried if at least two-thirds were covered with bedding.

Hole-board test. Exploratory behavior was assessed by the hole-board test that was performed according to Wang et al. (2016) and Martos et al. (2017). Mice were placed in the 40 cm × 40 cm Plexiglas arena containing a Plexiglas insertion with 16 equidistant 2-cm-wide holes. Mice were recorded for 30 min. The numbers and positions of head-dippings were scored by a blinded experimenter.

Response-based T-maze task. To test the ability to discriminate between a correct and incorrect body turn (left or right), we used a response-based T-maze task. We habituated the animals extensively before the training (Deacon and Rawlins, 2006), and we adapted the procedure as described by Okada et al. (2018). To perform in the task, mice were mildly food-restricted, and they were motivated by a sweetened

condensed milk, diluted in half of the original concentration with tap water. The volume of a single reward was 40 μ l. For the task, we used a cross-maze apparatus where one of the arms was always blocked so the apparatus formed a T-shape with one starting and two target arms. The blocked and the starting arm were opposite to each other, and their position was alternated so the starting positions were pseudo-randomly changing for each animal. During the habituation period, reward was placed in both target arms, and mice were taught to leave the starting arm and reach and consume the reward within 90 s. After the habituation, mice were moved to the acquisition phase where the reward was only placed in either left or right arm. The correct side was based on the actual starting position of the animal (see Fig. 7j), so it alternated between the arms, but the mouse was always required to take the same body turn. Once the mice reached the learning criterion in the acquisition phase (>50% in Cohort 1, 70% in Cohort 2), they were moved to the reversal phase where the correct body turn was switched. The mice that failed to reach the learning criterion during the acquisition were not moved to the reversal phase, but their acquisition data were included in the analysis. Because of control mice learning the task faster than expected in Cohort 1, we adjusted the learning criteria in Cohort 2 and the pooled data were expressed and analyzed as the percentage of control performance.

Instrumental and reversal learning in the operant box. Mice were tested using a standard operant chamber equipped with two fixed levers and a pellet dispenser (Med Associates). Mice were rewarded with chocolate-flavored cereal pellets (20 mg each, Bio-Serv). Throughout testing, mice received a maximum of 1 session per day, and they were usually tested 5 d per week. On day 1 of the pretraining, mice were habituated to the box for 10 min. No reward was administered during the session. After the session, four reward pellets per mouse were placed into the home cage for habituation to the reward. On day 2, a 10 min habituation to the box was performed again while four reward pellets were placed into the feeder. Only mice that consumed the pellets were moved to the next stage. On the third day, mice were placed in the box for 30 min while the dispenser automatically delivered 1 pellet every 2 min. Only mice that consumed all pellets were moved onto the next stage. On the last day of pretraining, mice were required to press any lever (left or right) to obtain a pellet reward. The criterion at this stage was to earn at least 30 rewards during a 30 min session while mice were allowed to earn maximum 40 rewards. During the acquisition stage, mice were required to press only the correct lever (either left or right; the correct side was chosen based on the last day of pretraining; it was the side that was less preferred) to obtain the reward. Pressing the incorrect lever was recorded, but it had no consequences. Mice were allowed to earn a maximum of 40 rewards during a 30 min session. The learning criterion required to move to the next stage was to earn all 40 rewards while maintaining at least 80% correct presses. After completing the acquisition phase, mice were subjected to two more identical sessions to ensure stable performance. In the following reversal phase, lever contingencies were switched so the previously correct lever became incorrect and vice versa. Again, mice were required to earn 40 rewards with at least 80% accuracy. After reaching this criterion, they were subjected to two more identical sessions.

IF

After the transcardial perfusion with 4% PFA in PBS, brains were extracted and postfixed overnight in PFA 4% at 4°C. Overnight incubations with sucrose 10% and 30% followed. Brains were cut with vibratome (Leica VT1000S) in 40 μ m sections for either on-slide IF or stored in the cryoprotective solution as free-floating. All procedures except for the primary antibody incubation were performed at room temperature. After the permeabilization step (1.2% Triton X-100 in PBS for 20 min), sections were washed in PBS for 10 min. For DARPP-32 staining, the permeabilization step has been replaced by three consecutive washes of 5 min in ethanol 50%, 70%, 50%. For blocking of the nonspecific binding, sections were incubated with 5% normal goat serum (NGS) in PBS for 1 h. Primary antibodies used were chicken or rabbit anti-GFP (Abcam, RRID:AB_300798, 1:1000, and Thermo Fisher Scientific, RRID:AB_2536526, 1:200, respectively), rabbit anti-c-Fos (Abcam, RRID:AB_

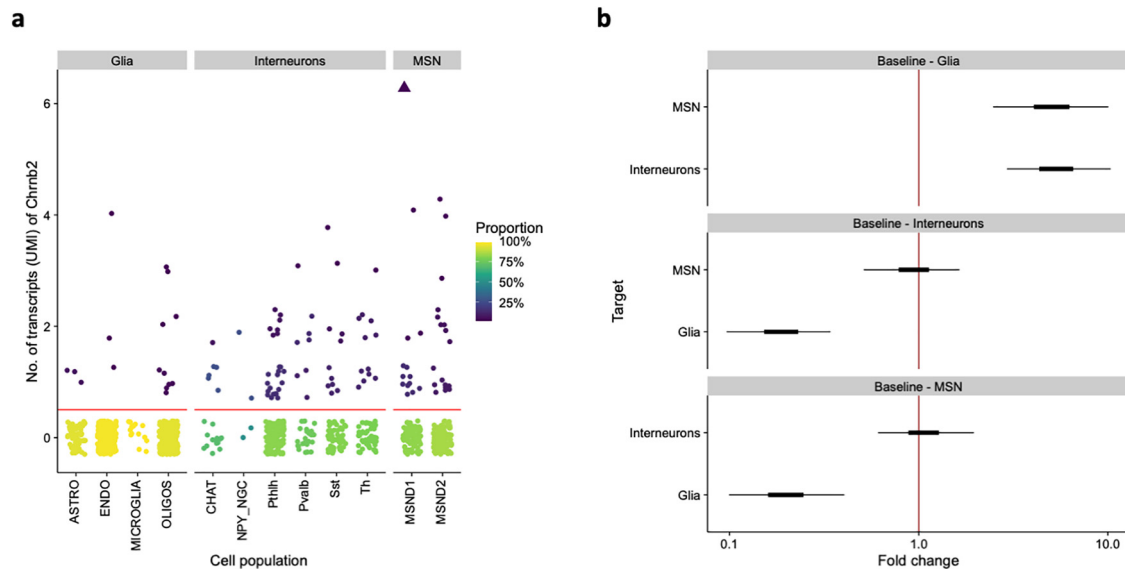


Figure 2. *Chrb2* expression in individual cell populations in the striatum. **a**, Expression of *Chrb2* across cell populations from (Muñoz-Manchado et al., 2018). Each point is a cell. Color represents the proportion of cells with the given number of transcripts in each population. The cells below the horizontal red line have no *Chrb2* transcripts. Triangle represents an outlier cell that had 13 reads. **b**, Differences between groups of cell populations as fitted by a Bayesian hierarchical GLM. Displayed are 50% (thick) and 95% (thin) posterior credible intervals for the difference of a given group (vertical axis) from a baseline group (subplot title). Fold change > 1 indicates that the group on the vertical axis has higher mean expression than the baseline group. ASTRO, astrocytes; ENDO, endothelial cells; OLIGOS, oligodendrocytes; CHAT, CINs; NPY_NGC, NPY-expressing neurogliaform INs; Pthlh, parathyroid hormone like hormone-expressing INs; Pvalb, parvalbumin-expressing INs; Sst, somatostatin-expressing INs; Th, TH-expressing INs; MSND1, D1-expressing MSNs; MSND2, D2-expressing MSNs.

2737414, 1:500) and goat anti-DARPP-32 (R&D Systems, RRID:AB_10641854, 1:500) and guinea pig anti-vesicular ACh transporter (VACHT) (1:5000) (Gras et al., 2008). They were diluted in PBS with 0.2% Triton X-100 and 2% NGS and incubated overnight at 4°C. The next day, sections were incubated with secondary antibodies (anti-chicken AlexaFluor-488, anti-rabbit AlexaFluor-594 and 680, anti-goat AlexaFluor-594, and anti-guinea pig AlexaFluor-594; Jackson ImmunoResearch Laboratories) in PBS with 0.2% Triton X-100 and 2% NGS, mounted on slides and coverslipped with Fluoroshield medium (Sigma). Images were acquired through Leica SP8 WLL MP confocal microscope, using HC PL FLUOTAR 5× and 10× and HC PL APO 40× objectives, and Andor Dragonfly 503-spinning disk confocal microscope (HCX PL APO 40× objective). Quantification of *c-Fos*-positive cells was performed with Fiji and CellProfiler software.

IF analysis of *c-Fos* expression

Quantification of *c-Fos*-positive cells was performed in *beta2-del* mice, in Cohorts 2–4 for a total of 40 animals divided into 4 experimental groups: 8 and 9 control mice obtained saline and amphetamine, respectively, 13 and 10 *beta2-del* mice received the same treatment. Two mice from the saline/*beta2-del* group and 1 mouse from the amphetamine/*beta2-del* group were excluded as outliers based on their locomotion or *c-Fos* expression data. For each animal, three confocal (40× objective) maximal projection pictures per hemisphere, spanning throughout the DS (AP 1.5 and AP 1.2 and AP 0.9, ML 1.5, DV 2.4) were quantified using Fiji (Schindelin et al., 2012) and CellProfiler software (Kamentsky et al., 2011). A pipeline was set up in CellProfiler, defining the global thresholding strategy with Otsu's method for the nuclei (Hoechst) and MoG for GFP and *c-Fos*. Objects with a typical diameter between 10 and 20 pixel units were counted. Clumped objects were distinguished by Laplacian of Gaussian method. Blue-thresholding module with intensity-calibrated resolution was used as mask for counting GFP and *c-Fos* objects. These values were controlled by manual multi-counting in Fiji. Positive cells for each marker were then expressed as percentage of the nuclei and averaged for each animal. Three animals from each experimental group were used for analyzing the colocalization of *c-Fos*-expressing cells with DARPP-32. The analysis was done by using custom macros in Python and ImageJ Macro Language with plugins (StarDist; JACoP; MorphoLibJ; 3D ImageJ Suite) (Bolte and Cordelières, 2006;

Olion et al., 2013; Legland et al., 2016; Schmidt et al., 2018) available for the Fiji software package to obtain suitable evaluation of the signal intensity throughout the *z* stacks. Seven control mice and 8 *beta2-del* mice were used for further evaluation of *c-Fos* expression in combination with VACHT and GFP expression. For each animal, two confocal *z*-stack pictures (63× objective) per hemisphere were quantified manually by using Fiji.

Data availability

Data generated in the study will be provided on request.

Results

mRNA coding for beta2 nicotinic subunit is expressed by specific groups of striatal INs, with CINs showing the highest level of expression

Although different subtypes of nAChRs are expressed by striatal neurons, the most common nicotinic subunit is likely the beta2 subunit coded by the *Chrb2* gene (Picciotto et al., 2000; Quik et al., 2009; Quik and Wonnacott, 2011; Eskow Jaunarajs et al., 2015). Therefore, to investigate the function of nAChRs in the mouse striatum, we decided to focus on this subunit. First, we used a previously published scRNA-seq study performed in the mouse striatum (Muñoz-Manchado et al., 2018) and reanalyzed the available data to assess the expression of the *Chrb2* gene, examining the dataset GSE97478 from Muñoz-Manchado et al. (2018). We found that the *Chrb2* mRNA is poorly expressed by all types of striatal neurons with little differences between individual groups (Fig. 2*a,b*). In all examined neuronal groups (MSNs and INs), a relatively large proportion of cells showed no *Chrb2* transcripts. However, in all these groups, there was a small proportion of cells expressing *Chrb2* to some extent (Fig. 2*a*). When comparing the mean expression of *Chrb2*, we could rule out substantial differences (fold change > 2) between groups of striatal neurons (Fig. 2*b*). Of note, non-neuronal cells showed minimal *Chrb2* expression, and the proportion of cells with zero transcripts was significantly higher and the mean expression

lower than those in the neuronal populations (Fig. 2*a,b*). The finding based on the scRNA-seq data was unexpected since most evidence in literature suggests that MSNs express considerably less (if any) nAChRs comparing to striatal INs. Therefore, we performed our own experiments using a different approach, allowing us to examine *Chrn2* expression simultaneously in multiple neuronal types *in situ*.

The phenotypes of the neurons expressing mRNA encoding the beta2 subunit of the nAChR (*Chrn2*) gene were analyzed by co-FISH in the mouse striatum (caudatum-putamen [CPU]) (Fig. 3). *Chrn2* mRNA was detected in scattered neurons all over the CPU (Fig. 3*a*). Several markers, including choline acetyltransferase (*Chat*, Fig. 3*b,c*), parvalbumin (*Pvalb*, Fig. 3*d*), neuropeptide Y (*Npy*, Fig. 3*e*), and somatostatin (*Sst*, Fig. 3*f*) for INs and D1 or D2 dopamine receptors (*Drd1* or *Drd2*, Fig. 3*g,h*) for MSNs were coanalyzed with *Chrn2*. As expected, all these markers were detected in the striatum with their specific expression profiles. Interestingly, *Chrn2* was detected in *Chat*⁺ neurons but also in *Chat*⁻ neurons (Fig. 3*b,c*), and the same observations were made for *Pvalb*, *Npy*, *Drd1*, and *Drd2* markers (Fig. 3*b–e,g,h*). *Chrn2* was virtually absent in *Sst*⁺ neurons (Fig. 3*f*). A quantitative analysis at 6 different bregma levels (rostral to caudal part of the CPU, 0.98; 0.74; 0.5; 0.26; 0.02; -0.22) revealed that *Chrn2* mRNA was expressed in the majority of *Chat*⁺ neurons (96%), but only in 24% of *Pvalb*⁺ and 5.5% of *Npy*⁺ neurons (Fig. 3*i*). *Chat*⁺ neurons expressing *Chrn2* gene were distributed over the whole striatum all along the rostro-caudal axis, whereas *Pvalb*⁺ and *Npy*⁺ neurons expressing *Chrn2* were located only in the dorsolateral part of the striatum. Expression of serotonin receptor 5HT_{3A} (*Htr3a* gene) was also analyzed as a marker for a presumably distinct population of INs (Faust et al., 2016). However, no or only very rare *Htr3a*⁺ cells were detected in the CPU, and no colocalization was detected with *Chrn2* mRNA in the cells (Fig. 3*k–m*). Interestingly, independent analyses of *Chrn2*-expressing cells in sections probed for different markers showed that 80%, 13%, and 7% of *Chrn2*-expressing neurons are also *Chat*⁺, *Pvalb*⁺, and *Npy*⁺, respectively, thus adding up to 100% of all *Chrn2*-expressing cells (Fig. 3*j*). Only 0.5% of *Drd1*⁺ neurons displayed *Chrn2* mRNA. Finally, the *Drd2*⁺ neurons that also displayed *Chrn2* gene were mostly large-sized, putatively representing CINs (Le Moine et al., 1990). In addition, the proportion of *Chrn2*⁺ neurons that were *Drd2*⁻ (20%) corresponded to the

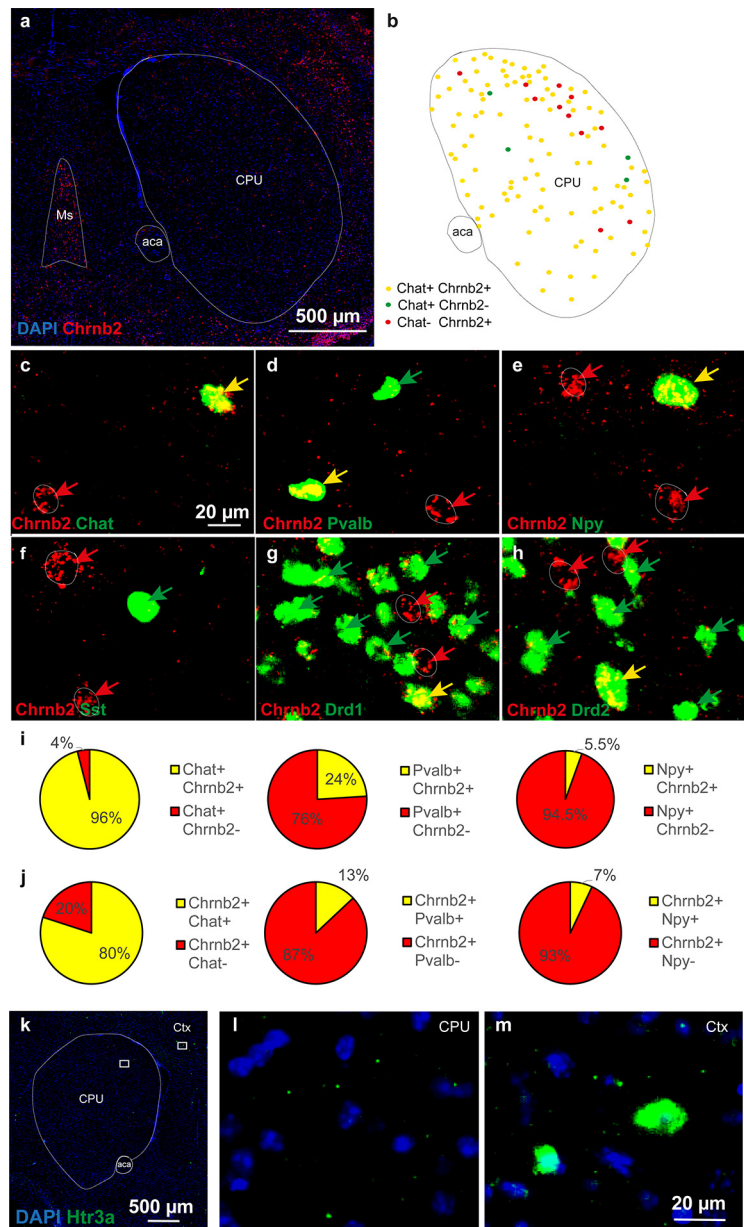


Figure 3. Double-labeling riboprobe FISH of serial sections identifying neuronal phenotypes expressing *Chrn2* gene in mouse striatum. **a**, Overview of *Chrn2* expression in the CPU at bregma 0.5. Red represents *Chrn2*. Blue represents DAPI. **b**, Schematic summary of findings mapping the extent of *Chrn2* and *Chat* overlap within CPU subnuclei. **c–h**, Closeups of codection of *Chrn2* (red) with the following (in green): (**c**) *Chat*, (**d**) *Pvalb*, (**e**) *Npy*, (**f**) *Sst*, (**g**) *Drd1*, and (**h**) *Drd2*. Arrows point to cells positive for one mRNA only (red or green) or double-positive (yellow arrows). **i**, Quantitative analysis of the proportion of *Chat*, *Pvalb*, or *Npy* gene-expressing neurons in the mouse striatum, displaying *Chrn2* mRNA. **j**, Quantitative analysis of the proportion of *Chrn2* gene-expressing neurons in mouse striatum displaying also *Chat*, *Pvalb*, or *Npy* mRNA. **i, j**, Percentage indicates the result of quantification per CPU from 3 male mice. A mean of 700, 1200, 520, and 830 for *Chat*, *Npy*, *Pvalb*, and *Sst* neurons, respectively, was analyzed per brain. **k–m**, *Htr3a*⁺ cells in mouse coronal brain section. **l**, Only minimum to none of *Htr3a*⁺ cells were found in the CPU. **m**, Several cells strongly positive for *Htr3a* are shown in the cortex. Ms, Medial septum; aca, anterior commissure; Ctx, cortex.

sum of the *Chrn2*⁺ neurons that were *Drd1*⁺ (*Chrn2*⁺/*Pvalb*⁺ and *Chrn2*⁺/*Npy*⁺).

AAV-Cre injection into the DS of beta2-flox/flox mice induces a selective deletion of the beta2 nicotinic subunit in striatal neurons

To investigate a functional role of beta2-containing nAChRs expressed by striatal INs, we deleted the beta2 subunit by injecting AAV-Cre virus into the DS of *beta2-flox/flox* mice carrying

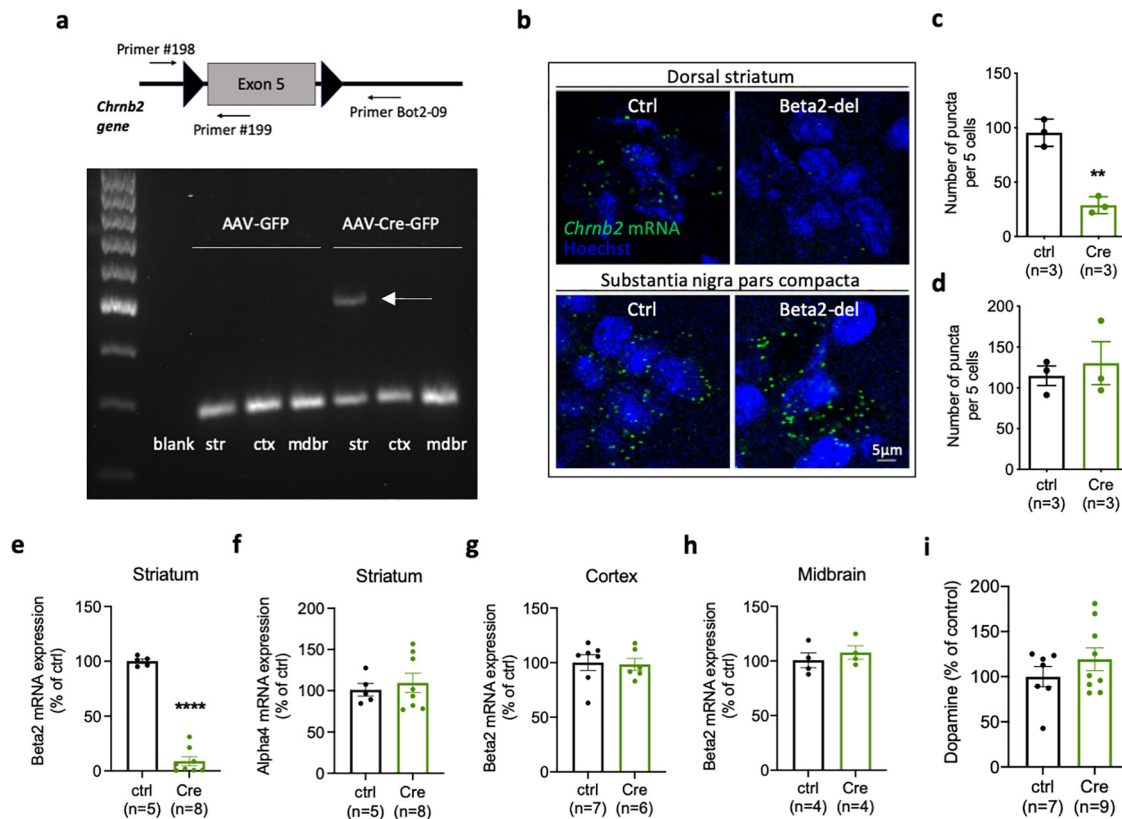


Figure 4. Striatal injection of AAV-Cre leads to a specific decrease of beta2 mRNA in the striatum of *beta2-flox/flox* mice. **a**, Top, Diagram showing exon 5 of the *Chrnb2* gene flanked by loxP sites in *beta2-flox/flox* mice. Locations of the three primers used in the ELFO analysis below are also indicated. Bottom, The ELFO analysis shows samples from two representative mice injected with AAV-GFP or AAV-Cre-GFP in the DS. Bottom row on the gel shows 200 bp products of #198 and #199 primers. Top additional band shows an additional 400 bp product of #198 and Bot2-09 primers indicating excision of exon 5. **b**, RNAscope visualization of *Chrnb2* mRNA in the DS and SNc in two representative mice injected with AAV-GFP or AAV-Cre-GFP. *Chrnb2* mRNA puncta are missing in the DS injected with Cre while the SNc of the same animal shows no decrease in puncta density. **c**, Quantification of *Chrnb2* mRNA puncta in the DS. $t_{(4)} = 7.824$, $p = 0.0014$, two-tailed t test. **d**, Quantification of *Chrnb2* mRNA puncta in the SNc. $t_{(4)} = 0.5321$, $p = 0.6228$, two-tailed t test. **e**, *Chrnb2* mRNA expression analyzed by qRT-PCR in striatal punches from AAV-expressing area of mice injected with AAV-GFP or AAV-Cre-GFP. $t_{(11)} = 16.95$, $p < 0.0001$, two-tailed t test. **f**, *Chrna4* mRNA expression analyzed by qRT-PCR in striatal punches from AAV-expressing area. $t_{(11)} = 0.5191$, $p = 0.6140$, two-tailed t test. **g**, **h**, *Chrnb2* mRNA expression analyzed by qRT-PCR in the cortex (**g**) and midbrain (**h**). Cortex: $t_{(11)} = 0.1788$, $p = 0.8613$; midbrain: $t_{(6)} = 0.7645$, $p = 0.4736$; two-tailed t test. **i**, Concentration of dopamine measured by ELISA in homogenates prepared from mice injected with AAV-GFP or AAV-Cre-GFP. $t_{(14)} = 1.106$, $p = 0.2874$, two-tailed t test. Number of samples used for analysis is indicated in graphs. Data are individual values and mean \pm SEM. str, Striatum; ctx, cortex; mdr, midbrain.

floxed exon 5 of the *Chrnb2* gene (Fig. 4a). The successful deletion of exon 5 was confirmed as an additional 400 bp fragment on agarose gel (Fig. 4a). Importantly, the deletion fragment was only present in striatal and not in midbrain samples which indicates that the virus did not travel retrogradely from the striatum into the SNc. We also measured beta2 mRNA by qRT-PCR, specifically targeting exon 5. We found a significant decrease in the level of beta2 mRNA isolated from striatal punches taken inside the AAV-expressing area of AAV-Cre-injected mice (95% CI for the difference between means $[-103.0; -79.35]$, $t_{(11)} = 16.95$, $p < 0.0001$, two-tailed t test). The expression of beta2 mRNA remained unaffected in the cortex and midbrain and the expression of the complementary nicotinic subunit alpha4 measured in striatal punches also did not change after beta2 deletion (Fig. 4e–h). Finally, we visualized the decrease of *Chrnb2* mRNA expression using RNAscope. The analysis showed a marked decrease of mRNA puncta in the striatum of AAV-Cre-injected mice compared with control animals (95% CI for the difference between means $[-90.17; -42.94]$, $t_{(4)} = 7.824$, $p = 0.0014$, two-tailed t test), while there was no difference in the SNc (Fig. 4b–d).

Midbrain DA neurons express their nAChRs on axonal terminals in the striatum where they control the release of striatal DA (Cachope et al., 2012; Threlfell et al., 2012). We used ELISA to measure DA concentrations in striatal homogenates from

control and AAV-Cre-injected mice, and we did not find any difference between the groups (Fig. 4i). However, our experimental approach cannot exclude more subtle changes in the release of striatal DA or changes limited to individual striatal subregions. Together, these experiments confirmed that the injection of the AAV-Cre virus caused a deletion of the beta2 subunit only at the site of injection. This was also confirmed by direct examination of the spread of the virus in both coronal and sagittal sections from brains of AAV5-Cre-injected animals. While we detected a strong viral expression in the DS (Fig. 5b,c), we detected negligible expression in the midbrain region. Specifically, in one sagittal section, we found 6 fluorescent nuclei in the SNc, suggesting that, while the retrograde transport of this virus is possible, it is rare, and likely does not contribute to a behavioral phenotype. Results of IF analysis of the viral expression and viral leakage into structures beyond the DS are schematically shown in Figure 5d.

Mice with a deletion of the beta2 subunit in striatal neurons show increased anxiety-like behavior and changes in social preference task

In the next part of the study, we wanted to examine whether beta2-containing nAChRs expressed by INs in the striatum play a role in controlling striatal-dependent behaviors. The striatum is a large structure with different subregions controlling different

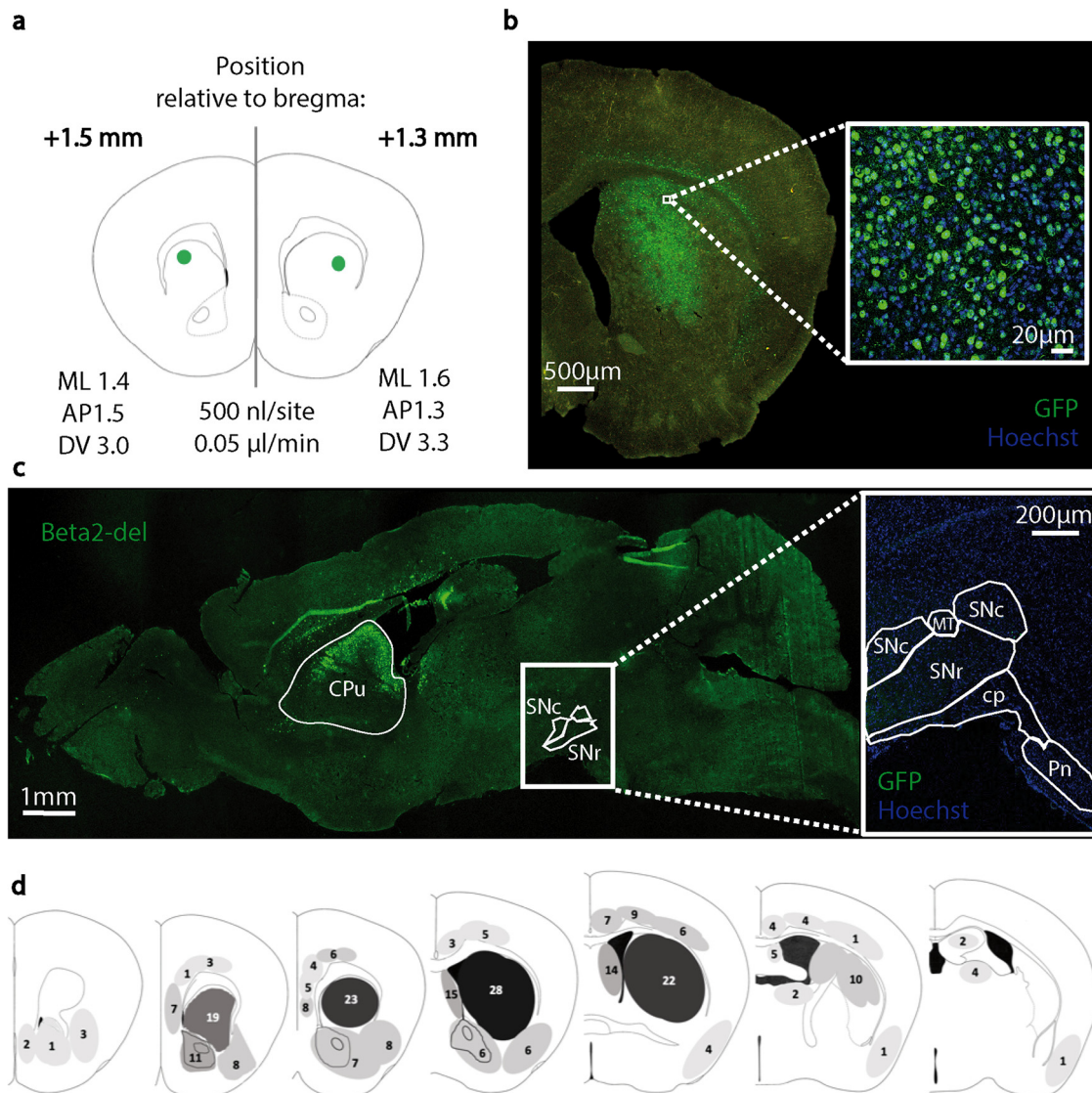


Figure 5. Expression of the AAV-Cre-GFP virus injected in the DS of *beta2-flox/flox* mice. **a**, Scheme of the viral injections, 2 sites per hemisphere (frontal section). **b**, A representative image of the injection extent in the DS. An enlarged image shows transduction by the AAV5 serotype used in the study. **c**, A sagittal brain section shows an expression of the AAV-Cre-GFP in the DS and an absence of the viral expression in the midbrain. **d**, Scheme of the degree of the AAV-Cre-GFP expression in mice used for behavioral testing. Shaded areas represent the extent of expression. Numbers in individual regions indicate the number of mice that showed viral expression in that region. A darker shade is proportional to a higher number of mice showing expression in the region. Two of the animals (of 32) used in behavioral tests died prematurely and were not included in the histologic analysis. ML, mediolateral; AP, anteroposterior; DV, dorsoventral; SNc, substantia nigra pars compacta; SNr, substantia nigra pars reticulata; MT, medial terminal nucleus; cp, cerebral peduncle; Pn, pontine nuclei.

functions. In our study, we primarily focused on the DS, including both medial and lateral parts. The beta2-containing nAChRs were previously shown to play a role in fundamental behaviors in mice, including feeding, motivation, and sleep/wake behavior (Léna et al., 2004; Konsolaki et al., 2016; Dezfuli et al., 2020). We subjected a group of mice with the beta2 deletion in the DS (further referred to as *beta2-del* mice) and control mice to a battery of behavioral tasks that are known to depend on striatal functions or, in some cases, on nAChRs. However, investigating these domains did not reveal any significant difference between control and *beta2-del* mice (Fig. 6*a,b,i,j*; see Fig. 8*f,g*).

We also measured spontaneous locomotion in the open field in 2 consecutive days, thus probing activity in novel and familiar environment. Control and *beta2-del* mice were not significantly different, although there was a trend to hyperactivity on day 1 (novel environment) and the groups were very similar on day 2 (familiar environment) (day vs group interaction: 95% CI

[−0.6509; 16.20], $F_{(1,59)} = 3.409$, $p = 0.0699$; two-way ANOVA) (Fig. 6*c,d*; see Fig. 8*h*). When we analyzed the time mice spent in the center versus in the edges of the open field arena, we found that *beta2-del* mice spent less time in the center compared with controls (main effect of group: 95% CI for the difference between means [−8.475; −1.676], $F_{(1,59)} = 8.925$, $p = 0.0041$; two-way ANOVA), namely, during the first day of the test (difference between means on day 1: 95% CI [−12.0; −3.122], $p = 0.0004$; day 2: 95% CI [−7.028; 1.845], $p = 0.3412$; Sidak's post-test) (Fig. 6*e*; see Fig. 8*a,i*). Spending less time in the central part of a novel environment indicates an increase in the anxiety-like behavior. Therefore, we used additional tasks to examine the anxiogenic effect of a beta2 deletion. The EPM did not reveal any effect of the beta2 deletion (Fig. 6*f*; see Fig. 8*k*), whereas in the light/dark transition task, we found that the *beta2-del* mice spend slightly but significantly less time in the light part of the apparatus compared with controls (95% CI for the difference between means

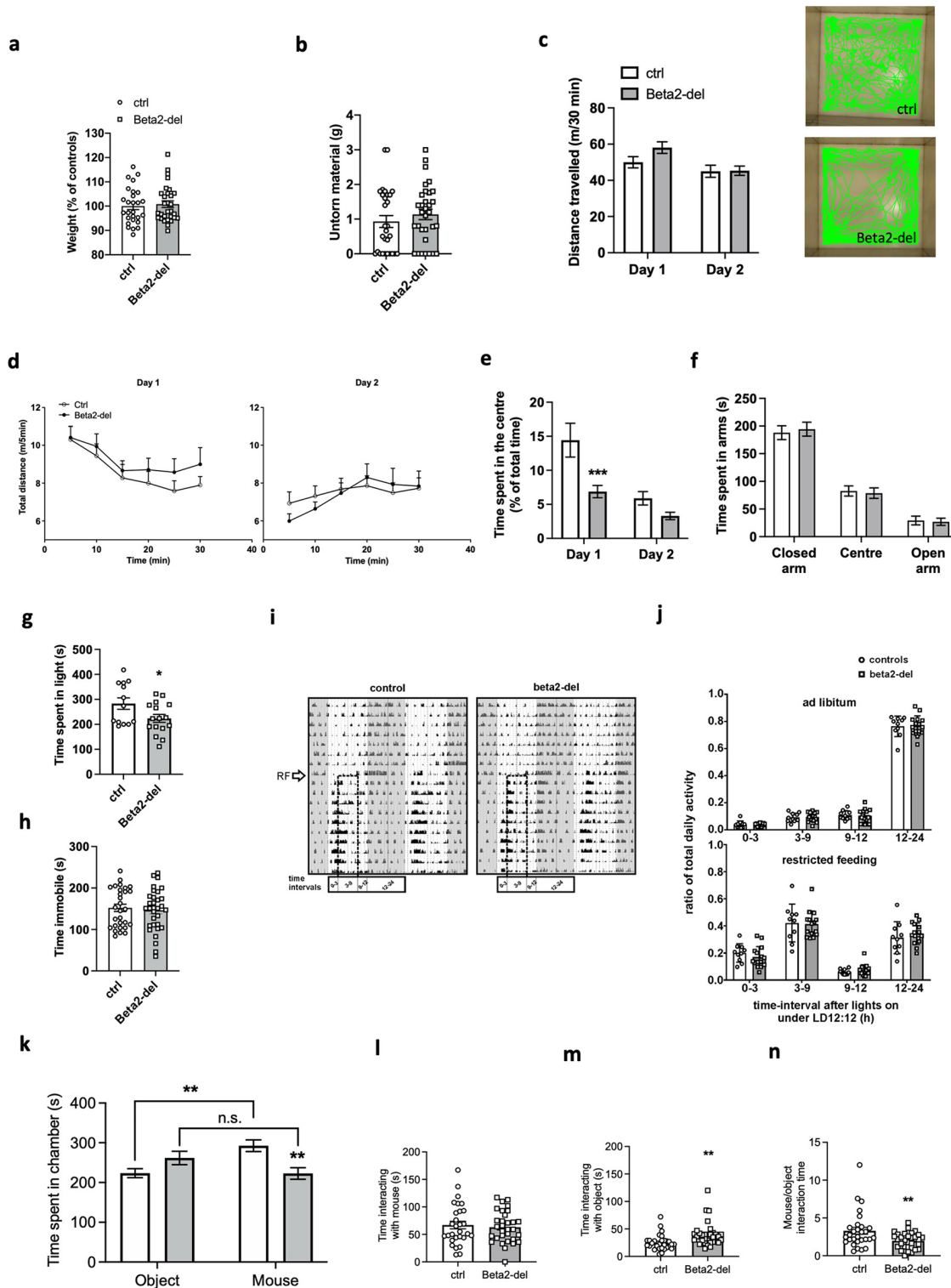


Figure 6. *Beta2-del* mice show increased anxiety-like behavior and changes in the social task. **a**, Weight of *beta2-del* and control mice 1 month after surgery. $n = 30$, $n(\text{ctrl}) = 27$. $t_{(55)} = 0.4069$, $p = 0.6857$, two-tailed t test. **b**, The amount of nestlet material left untorn in the nest building task. $n = 32$, $n(\text{ctrl}) = 29$. 95% credible interval for difference in untorn material proportion (%) [−0.6; 20], Bayesian GLM. **c**, Left, Distance traveled during 30 min in the open field task measured on 2 consecutive days. $n = 32$, $n(\text{ctrl}) = 29$. Effect of group: $F_{(1,59)} = 1.255$, $p = 0.2672$; effect of day: $F_{(1,59)} = 17.81$, $p < 0.0001$; group versus day interaction: $F_{(1,59)} = 3.409$, $p = 0.0699$; two-way ANOVA. Right, Representative track records of a control and *beta2-del* mouse during the first day in the open field. Note the lower preference for the central part of the arena by the *beta2-del* mouse. **d**, Locomotor activity in open field divided into 5 min time bins, measured on day 1 (left) and day 2 (right). **e**, Time spent in the center of the open field arena measured on 2 consecutive days. $n = 32$, $n(\text{ctrl}) = 29$. Effect of group: $F_{(1,59)} = 8.925$, $p = 0.0041$; effect of day: $F_{(1,59)} = 38.56$, $p < 0.0001$; group versus day interaction: $F_{(1,59)} = 6.494$, $p = 0.0134$; two-way ANOVA. **f**, Time spent in the open and closed arms of the EPM apparatus. $n = 31$, $n(\text{ctrl}) = 26$. Effect of group: $F_{(1,65)} = 0.000$, $p > 0.999$; effect of arm: $F_{(2,165)} = 138.6$, $p < 0.0001$; genotype versus arm interaction, $F_{(2,65)} = 0.1530$, $p = 0.8583$; two-way ANOVA. **g**, Time spent in the light part of the arena during the light/dark task. $n = 16$, $n(\text{ctrl}) = 13$. $t_{(27)} = 2.184$, $p = 0.0378$; two-tailed t test. **h**, Time spent immobile during the FST task. $n = 32$, $n(\text{ctrl}) = 29$. 95% CI for *beta2-del*/controls ratio [0.88; 1.22], $p = 0.658$, GLM. **i**, Representative double-plotted locomotor activity records (actograms) of 1 control (left) and 1 *beta2-del* (right) mouse. The mice were maintained in the original light/dark cycle (gray area represents darkness), and then they were exposed to a restricted feeding (RF) regimen (arrow) for 10 d.

[−115.1; −3.595], $t_{(27)} = 2.184$, $p = 0.0378$; two-tailed t test) (Fig. 6g; see Fig. 8b). Finally, we saw no difference between the control and *beta2-del* mice in immobility time during the FST used for evaluation of behavioral despair (Fig. 6h; see Fig. 8j).

Previously, it has been shown that social behavior depends on different types of INs in the DS (Rapanelli et al., 2017). For the assessment of social behavior in *beta2-del* mice, we used the social preference task (Fig. 6k–n; see Fig. 8c,d,l–o). In contrast to control animals who significantly preferred the mouse chamber, the *beta2-del* mice did not show this preference and the time they spent in with a mouse or an object did not differ (chamber vs group interaction, 95% CI [49.63; 166.4], $F_{(1,116)} = 13.43$, $p = 0.0004$; two-way ANOVA) (Fig. 6k; see Fig. 8l). When we directly compared the time that the two groups spent in the social chamber, we found a significant decrease in *beta2-del* mice (95% CI for the difference between means [−117.1; −22.64], $p = 0.0022$, Sidak's post-test) (Fig. 6k). To enhance our understanding of the behavior occurring during the task, we analyzed time that the two groups of mice spent directly interacting (sniffing or pawing) with the social and non-social stimulus. Surprisingly, the time spent interacting with the mouse did not differ between controls and *beta2-del* mice (95% CI for the difference between means [−20.95; 13.14], $t_{(58)} = 0.4590$, $p = 0.6480$, two-tailed t test) (Fig. 6l; see Fig. 8m). In contrast, the *beta2-del* mice showed notably longer time spent examining the non-social stimulus (95% CI for *beta2-del*/controls ratio [1.19; 2.1], $p = 0.003$, GLM) (Fig. 6m; see Fig. 8c,n). Thus, the lower sociability ratio in the *beta2-del* mice was purely driven by an increased object exploration (Fig. 6n; see Fig. 8d,o). In summary, the *beta2-del* mice showed no changes in weight, nest building, food-anticipatory activity, locomotion, and depressive-like behavior while they showed an increased anxiety-like behavior in two of three tests. In addition, the most marked behavioral change in *beta2-del* mice was an impairment in social preference task driven by a relatively higher interest in inanimate objects compared with social stimuli.

Deletion of the beta2 nicotinic subunit in striatal neurons impairs response discrimination learning but has no effect on cognitive flexibility

In the next set of experiments, we focused on evaluating of cognitive functions in *beta2-del* mice. Striatal ACh is indispensable for intact cognitive flexibility (Prado et al., 2017; Favier et al.,

2020), and nAChRs expressed by striatal INs have been also hypothesized to play a role in this cognitive domain. Thus, we used multiple tests to investigate cognitive flexibility and goal-directed behavior. These tests included cued MWM for goal-directed behavior, grooming test, marble burying test, and hole board test for compulsive-like and repetitive behavior and lever-pressing task in the operant box for reversal learning, but we did not find a significant alteration in any of them (Fig. 7a–h). In addition, episodic-like memory was not impaired in the *beta2-del* mice as documented by NOR test (Fig. 7i). Finally, we trained *beta2-del* mice in a response-based T-maze task to examine their egocentric navigation, discrimination, and reversal learning (Figs. 7j–l, 8e). In this task, mice were trained to navigate to a reward whose position was dependent on a mouse's body turn. Two different starting arms of the maze were pseudo-randomly alternated so that mice would not learn the position of the reward from the spatial cues (Fig. 7j). In the acquisition phase of the task, mice were trained to make the correct body turn; and in the following reversal phase, the correct turn was changed to the opposite direction. We found that *beta2-del* mice needed significantly more training sessions to reach the accuracy criteria during the acquisition phase of the T-maze task (mean percentage of the control values \pm SEM in *beta2-del*: 178.8 ± 5.9 , 95% CI for the difference between means [11.76; 145.9], $t_{(13,96)} = 2.521$, $p = 0.0245$; Welsh's t test) (Figs. 7k, 8e). In contrast, the reversal phase did not show an impairment in *beta2-del* mice. Instead, the data were more consistent with a better performance in *beta2-del* animals (mean percentage of the control values \pm SEM in *beta2-del*: 78.4 ± 7.2 , 95% CI for the difference between means [−51.69; 8.489], $t_{(20)} = 1.497$, $p = 0.1499$, two-tailed t test) (Fig. 7l). In summary, cognitive tests showed no impairment of cognitive flexibility in *beta2-del* mice, but they identified the impairment of the initial discrimination learning in the egocentric navigation-based T-maze task.

Deletion of the beta2 nicotinic subunit increases c-Fos expression in the DS and leads to a higher sensitivity to amphetamine

The FISH analysis showed that beta2-containing nAChRs are predominantly expressed by striatal INs, and their expression by MSNs is negligible. Based on this finding, we asked whether the beta2 deletion would lead to a decreased activity of striatal INs and what would be the ultimate effect on the activity of MSNs. To answer this question, *beta2-del* and control mice received intraperitoneal injection of either saline or amphetamine (Fig. 9a). Following the injection, we measured locomotion as a behavioral marker of striatal activity, and we also evaluated c-Fos expression in the DS as a biochemical correlate of neuronal activity. The comparison of controls and *beta2-del* mice during the habituation period (before injection) revealed a significantly higher locomotor activity in the *beta2-del* (95% CI for the difference between means [4.787; 27.29], $t_{(42)} = 2.877$, $p = 0.0063$, two-tailed t test) (Figs. 8p, 9b,d). When we analyzed the activity of mice after the injection, we found a significant effect of amphetamine (main effect of treatment: 95% CI [58.03; 154.9], $F_{(1,40)} = 19.75$, $p < 0.0001$, two-way ANOVA) and no effect of group or interaction (Figs. 8q, 9c,d). When further examined with post-tests, we found a marked difference between the saline- and amphetamine-injected *beta2-del* mice (95% CI [52.83; 225.8], $p = 0.0006$, Tukey's multiple comparisons test) and no difference between the saline- and amphetamine-injected controls, possibly because of older age of the experimental animals (8 months; see Fig. 1).

←

Dashed rectangle represents the time of food availability during 6 h centered to the middle of the light phase. Time intervals during which the activity was compared between the controls and the *beta2-del* mice are shown at the bottom of the actograms. $n = 15$, $n(\text{ctrl}) = 10$. **j**, Comparison of locomotor activity of the control (circles, open column) and the *beta2-del* (squares, gray column) mice under *ad libitum* (top) and restricted feeding (bottom) conditions as assessed in four intervals during the 24 h cycle depicted in **i**. The activity is expressed as the ratio of total daily activity of each mouse. Data were analyzed by multiple t test: top, 0–3, $p = 0.7522$; 3–9, $p = 0.7941$; 9–12, $p = 0.8045$; 12–24, $p = 0.8953$; bottom, 0–3, $p = 0.3174$, 3–9, $p = 0.8551$, 9–12, $p = 0.4827$, 12–24, $p = 0.4526$. **k**, Time spent in the individual chambers of the apparatus during the social preference task. $n = 32$. $n(\text{ctrl}) = 28$. Effect of group: $F_{(1,116)} = 1.158$, $p = 0.2842$; effect of chamber: $F_{(1,116)} = 1.041$, $p = 0.3098$; group versus chamber interaction: $F_{(1,116)} = 13.43$, $p = 0.0004$; two-way ANOVA. **l**, Time spent directly interacting with a juvenile mouse during the social preference task. $t_{(58)} = 0.4590$, $p = 0.6480$, two-tailed t test. **m**, Time spent directly interacting with an inanimate object during the social preference task. $p = 0.003$, GLM. **n**, Sociability in *beta2-del* and control mice expressed as a ratio of time spent interacting with a mouse versus time spent interacting with an object. $p = 0.009$; GLM. Data are mean \pm SEM. In selected tasks, we also correlated main behavioral parameters to the extent of AAV expression in the DS (see Fig. 8a–e). In tasks that were performed in all Cohorts 1–4, we analyzed performance of mice divided according to the age (Cohorts 1&2 vs Cohorts 3&4) (see Fig. 8f–g).

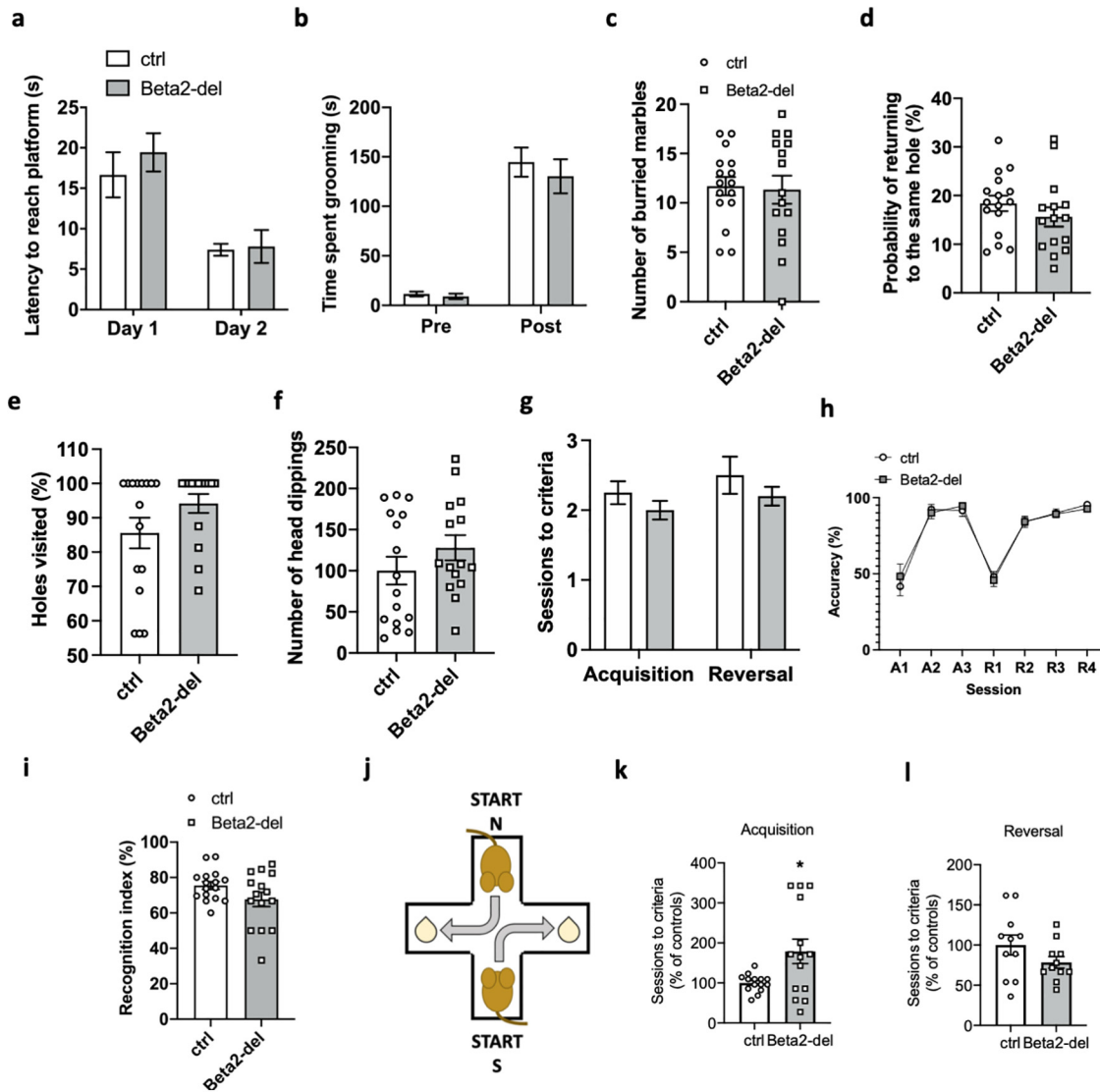


Figure 7. *Beta2-del* mice show a deficit in the acquisition of the T-maze task, but they have no impairment of cognitive flexibility. **a**, Latency to reach a visible platform in the cued-MWM task. $n = 15$, $n(\text{ctrl}) = 16$. Effect of group: $F_{(1,29)} = 0.3785$, $p = 0.5432$; effect of day: $F_{(1,29)} = 48.16$, $p < 0.0001$; group versus day interaction: $F_{(1,29)} = 0.6274$, $p = 0.4347$; two-way ANOVA. **b**, Time spent grooming during the grooming test before and after spraying the mice with water. $n = 15$, $n(\text{ctrl}) = 16$. Effect of group: $F_{(1,58)} = 0.5290$, $p = 0.4699$; effect of phase: $F_{(1,58)} = 123.5$, $p < 0.0001$; group versus phase interaction: $F_{(1,58)} = 0.2765$, $p = 0.6010$; two-way ANOVA. **c**, Number of buried marbles during the marble burying test. $n = 15$, $n(\text{ctrl}) = 16$. $t_{(29)} = 0.2103$, $p = 0.8349$, two-tailed t test. **d**, The probability of returning to the same hole during the hole-board test. $n = 15$, $n(\text{ctrl}) = 16$. $t_{(29)} = 1.611$, $p = 0.1180$, two-tailed t test. **e**, The percentage of visited holes (of 16) during the hole-board test. $t_{(29)} = 1.611$, $p = 0.1180$, two-tailed t test. **f**, The total number of head dippings during the hole-board test. $p = 0.27$, GLM. **g**, Number of sessions needed to reach criteria during the acquisition and reversal phase of the instrumental task. $n = 11$, $n(\text{ctrl}) = 8$. $F_{(1,33)} = 2.488$, $p = 0.1243$, mixed-effects model. **h**, Percentage of correct presses during different stages of a simple instrumental task in the operant box. Effect of group: $F_{(1,17)} = 0.01091$, $p = 0.9180$; effect of session: $F_{(2,537,41,44)} = 57.05$, $p < 0.0001$; group versus session interaction: $F_{(6,98)} = 0.3622$, $p = 0.9011$; mixed-effects model. **i**, Recognition index in the NOR test. $n = 15$, $n(\text{ctrl}) = 16$. $t_{(21,56)} = 1.708$, $p = 0.1021$, Welch's t test. **j**, Diagram represents two alternating starting positions in the response-based T-maze task and the respective location of the reward. **k**, Number of sessions needed to reach learning criteria during the acquisition phase of the T-maze task expressed as percentage of control performance. $n = 14$, $n(\text{ctrl}) = 14$. $t_{(13,96)} = 2.521$, $p = 0.0245$; Welch's t test. **l**, Number of sessions needed to reach learning criteria during the reversal phase of the T-maze task expressed as percentage of control performance. $n = 11$, $n(\text{ctrl}) = 8$. $t_{(20)} = 1.497$, $p = 0.1499$, two-tailed t test. Data are mean \pm SEM. In selected tasks, we also correlated main behavioral parameters to the extent of AAV expression in the DS (see Fig. 8*a–e*). In tasks that were performed in all Cohorts 1–4, we analyzed performance of mice divided according to the age (Cohorts 1&2 vs Cohorts 3&4) (see Fig. 8*f–q*).

In addition to measuring locomotion as a behavioral marker of MSN activity, we also evaluated c-Fos expression in the DS. Similar to the analysis of locomotor activity, we found a significant effect of amphetamine (main effect of treatment: 95% CI [0.5088; 2.307], $F_{(1,33)} = 10.15$, $p = 0.0031$, two-way ANOVA). In addition, there was an effect of beta2 deletion (main effect of group: 95% CI [0.1795; 1.977], $F_{(1,33)} = 5.958$, $p = 0.0202$; two-way ANOVA), and post-tests showed only a significant difference between the saline- and amphetamine-injected *beta2-del* mice (95% CI [0.2063; 3.452], $p = 0.0222$, Tukey's multiple

comparisons test) (Fig. 9*e,g*). Given the similarity of the locomotion and c-Fos expression data, we decided to test whether locomotor activity is correlated with the level of c-Fos expression. Indeed, the distance traveled after injection was positively correlated with the percentage of c-Fos-expressing cells in the DS (Fig. 9*f*), suggesting that both parameters can be used as indicators of striatal activity. In summary, *beta2-del* mice showed an increase in both behavioral and biochemical marker of striatal activity. The striatum is composed of two different types of MSNs with antagonistic effect on locomotor activity and several types of INs

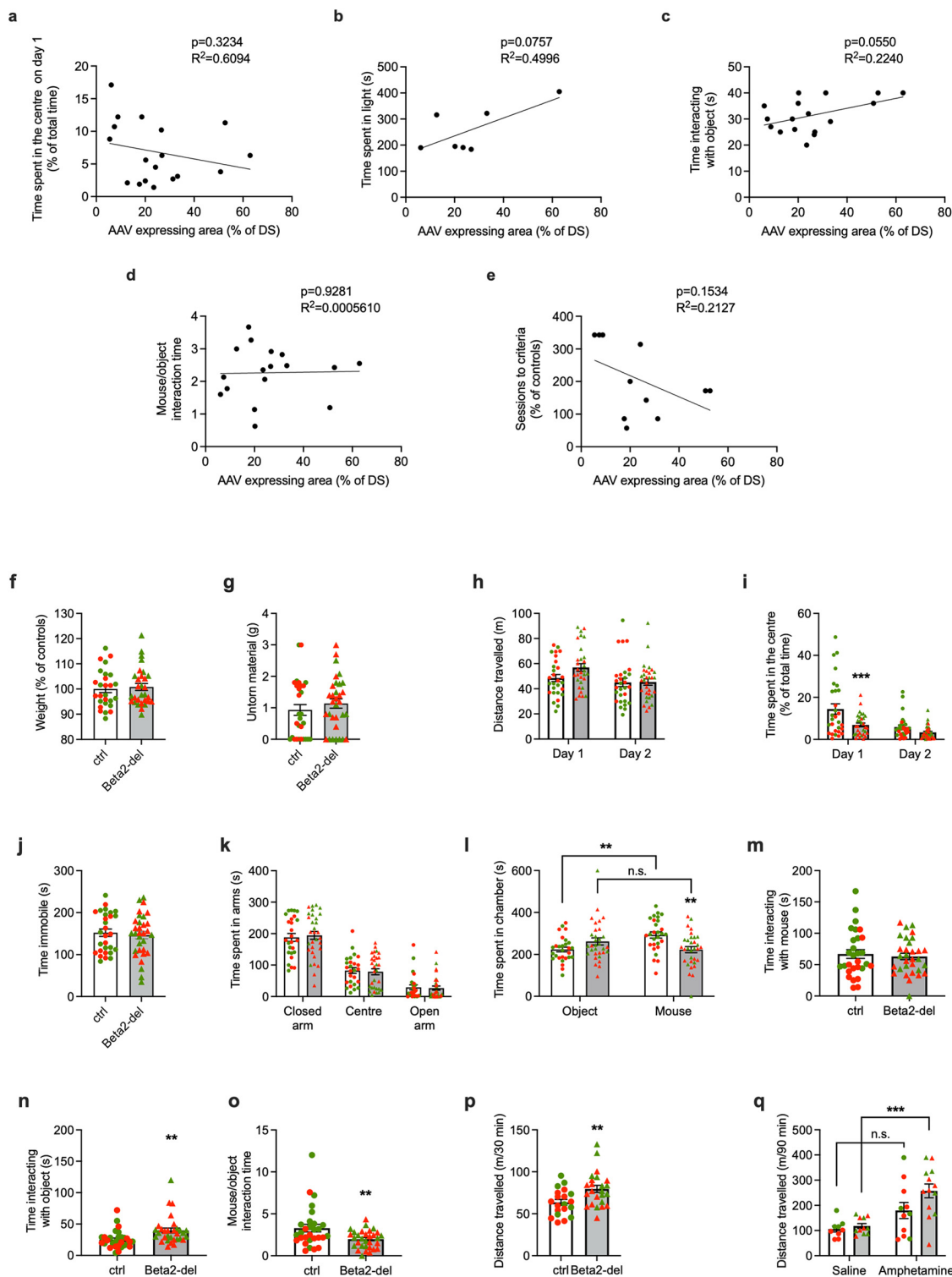


Figure 8. Additional analysis of selected behavioral tasks. **a–e**, Main parameters of selected behavioral tasks correlated to AAV expression in the DS. The individual parameters are **(a)** time spent in the center (%) during the open field test on day 1, **(b)** time spent in light (s) during the light/dark task, **(c)** time interacting with object (s) during the social preference test, **(d)** mouse/object interaction time (ratio) during the social preference test, and **(e)** number of sessions needed to reach performance criteria in the acquisition phase of the T-maze task. None of the parameters shows a significant correlation with the AAV expression, although the correlation almost reaches significance in **c**. **f–q**, Graphs represent split performance for Cohorts 1&2 versus Cohorts 3&4. Individual performances corresponding to mice in Cohorts 1&2 (green circles and triangles represent controls and *beta2-del*, respectively) and Cohorts 3&4 (red circles and triangles represent controls and *beta2-del*, respectively) are shown. Only tests that were performed in both cohorts are shown: **(f)** weight after surgery, **(g)** nest building test, **(h,i)** locomotion in the open field, **(j)** FST, **(k)** EPM, **(l–o)** social preference task, and **(p,q)** locomotion in amphetamine experiment before **(p)** and after **(q)** injection. When performance of ctrl and *beta2-del* mice was analyzed separately for Cohorts 1&2 versus Cohorts 3&4, only the difference in “Time interacting with object” **(n)** reached the significance in both cohorts before pooling the data.

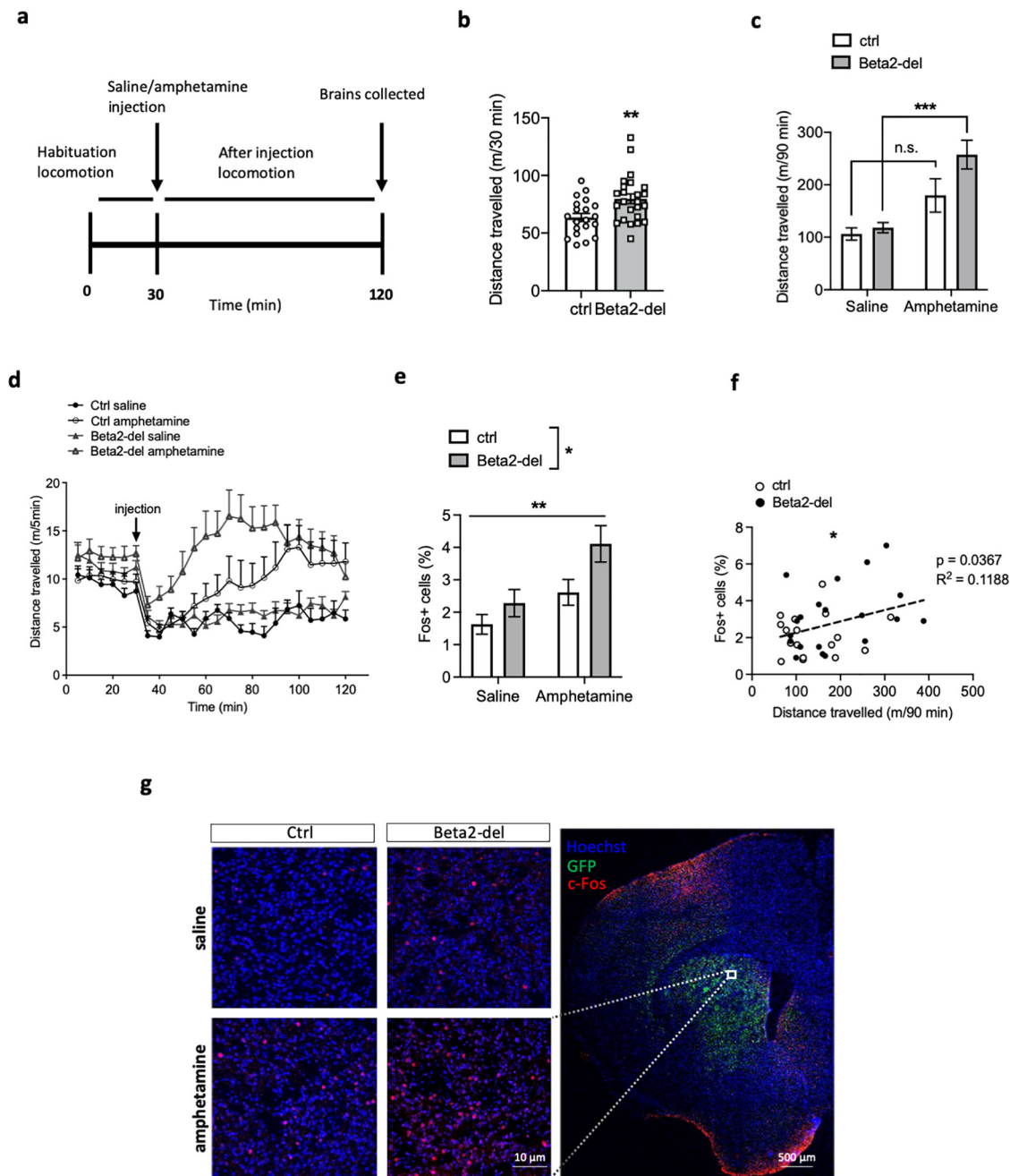


Figure 9. *Beta2-del* mice are hyperactive and show higher amphetamine-induced *c-Fos* expression compared with controls. **a**, Diagram showing the experimental design. **b**, Distance traveled during the 30 min of habituation (pre-injection) in the open field. $n = 24$, $n(\text{ctrl}) = 20$. $t_{(42)} = 2.877$, $p = 0.0063$, two-tailed t test. **c**, Distance traveled in the open field for the 90 min following an acute saline or amphetamine injection. $n(\text{saline/amphetamine}) = 11/13$, $n(\text{ctrl; saline/amphetamine}) = 9/11$. Effect of group: $F_{(1,40)} = 3.519$, $p = 0.068$; effect of treatment: $F_{(1,40)} = 19.75$, $p < 0.0001$; group versus treatment interaction: $F_{(1,40)} = 1.886$, $p = 0.1773$; two-way ANOVA. **d**, Locomotion during the amphetamine experiment divided into 5 min time bins. We also analyzed distance traveled before and after injection in individual cohorts of mice divided according to the age (Cohorts 1&2 vs Cohorts 3&4) (see Fig. 8*p,q*). **e**, Analysis of *c-Fos* expression in the DS of *beta2-del* and control mice injected either with saline or amphetamine. $n(\text{saline/amphetamine}) = 11/9$, $n(\text{ctrl; saline/amphetamine}) = 8/9$. An average of 1000 nuclei per picture were analyzed in 6 brain sections per mouse. Effect of group: $F_{(1,33)} = 5.958$, $p = 0.0202$; effect of treatment: $F_{(1,33)} = 10.15$, $p = 0.0031$; group versus treatment interaction: $F_{(1,33)} = 0.9106$, $p = 0.3469$; two-way ANOVA. **f**, Distance traveled after injection correlated to *c-Fos* expression. **g**, Right, Representative section counterstained with Hoechst showing GFP and *c-Fos* expression. White square represents a typical area in the DS that was used for *c-Fos* analysis. Left, Representative images counterstained with Hoechst showing baseline and amphetamine-induced *c-Fos* expression in *beta2-del* and control animals. Data are mean \pm SEM.

which effect on locomotion is largely unknown. To obtain more information on the identity of *c-Fos*-expressing neurons associated with the increased locomotion, we stained striatal sections in a subgroup of ctrl and *beta2-del* mice with the antibody against dopamine- and cAMP-regulated neuronal phosphoprotein (DARPP-32), a marker of MSNs (Fig. 10*a*). As expected, most of the *c-Fos*-expressing neurons were also stained for the

DARPP-32, as MSNs form ~95% of all striatal neurons. However, between 5% and 10% of *c-Fos*-expressing neurons in all examined sections were DARPP-32 negative, presumably representing activated striatal INs (Fig. 10*a,b*). The proportion of DARPP-32 negative/*c-Fos*-positive neurons was similar in all experimental groups, indicating that both the beta2 deletion and the amphetamine treatment increased the activity in both MSNs

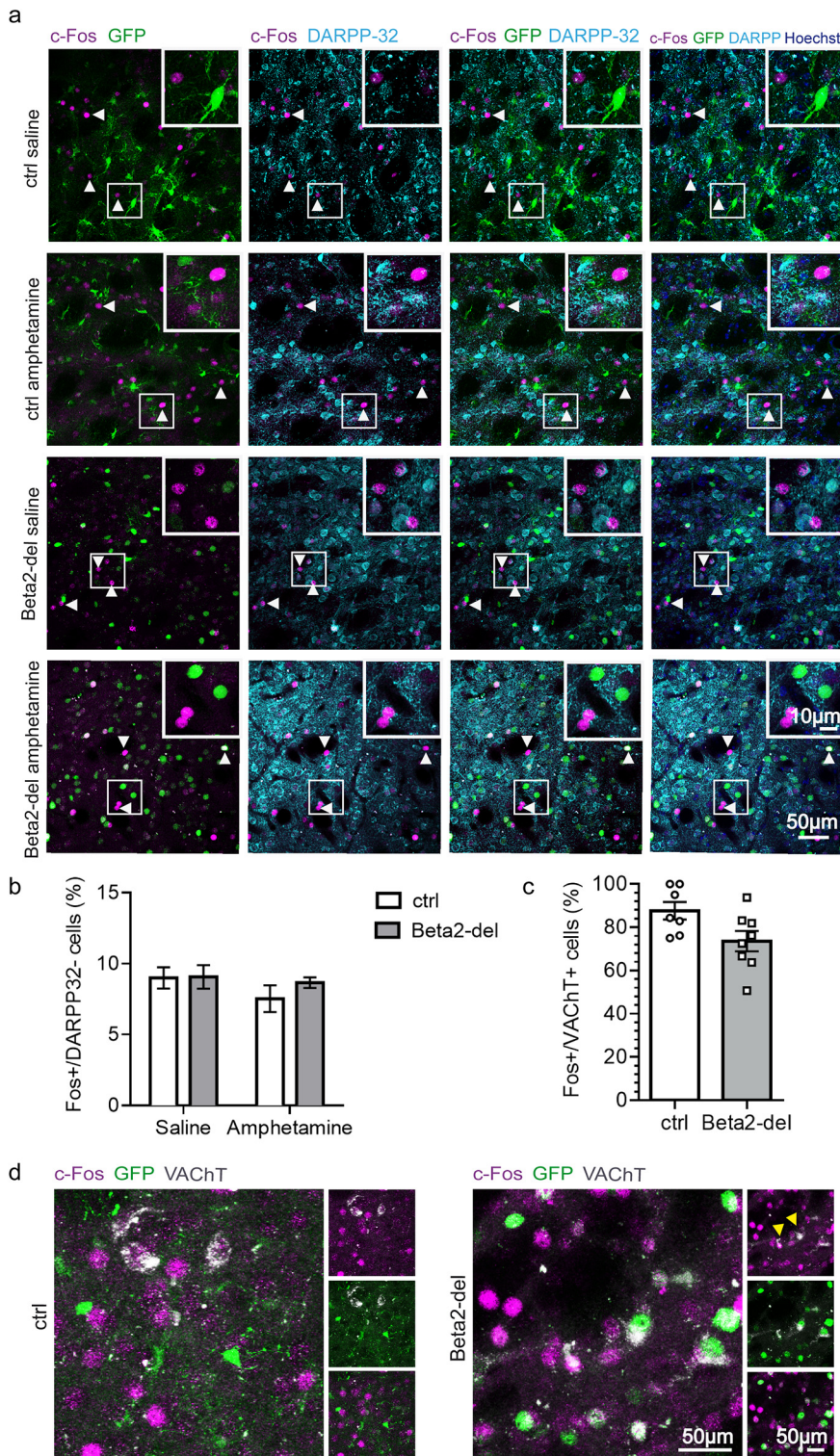


Figure 10. c-Fos-expressing neurons include both DARPP-32⁺ MSNs and DARPP-32⁻ INs. **a**, Representative images showing baseline and amphetamine-induced c-Fos expression in *beta2-del* and control animals in combination with DARPP-32 and GFP staining (indicating the AAV-expressing area with presumed beta2 deletion). From the left, Merged images represent the following: c-Fos double labeling with GFP; c-Fos double labeling with DARPP-32; c-Fos triple labeling with GFP and DARPP-32; the combination of the three markers over Hoechst counterstain for nuclei. White arrowheads highlight c-Fos-positive cells, not expressing DARPP-32. White squares represent closeups on the c-Fos⁺/DARPP-32⁻ cells. **b**, Number of c-Fos⁺ and DARPP-32⁻ cells expressed as percentage of all c-Fos⁺ neurons in *beta2-del* and control mice injected with either saline or amphetamine. $n(\text{saline}/\text{amphetamine}) = 3/3$, $n(\text{ctrl}; \text{saline}/\text{amphetamine}) = 3/3$. An average of 25 c-Fos⁺, DARPP-32⁻ neurons were analyzed in two brain sections per mouse. Effect of group: $F_{(1,8)} = 0.6286$, $p = 0.4507$; effect of treatment: $F_{(1,8)} = 1.541$, $p = 0.2497$; group versus treatment interaction: $F_{(1,8)} = 0.4934$, $p = 0.5023$; two-way ANOVA. **c**, Number of c-Fos⁺ neurons out of all VACHT⁺ neurons in control and *beta2-del* mice. Saline and amphetamine-injected mice were pooled together in each group. $n(\text{ctrl}) = 7$, $n(\text{beta2-}$

and INs (Fig. 10*b*). Finally, we hypothesized that, among the different types of striatal INs, those with significant beta2 deletion (i.e., CINs) should show a decrease in c-Fos expression. We tested this hypothesis by triple staining against GFP, c-Fos, and VACHT, a marker for CINs. Analysis of c-Fos and VACHT labeling revealed that percentage of c-Fos-positive neurons out of all VACHT-positive neurons was lower in *beta2-del* mice compared with controls, although because of low number of CINs and between-mice variability, the evidence is not completely conclusive (95% credible interval for the odds ratio between ctrl and *beta2-del* [0.09; 1.02], generalized linear mixed model) (Fig. 10*c,d*).

Discussion

Although ACh is widely accepted as a key modulator of striatal signaling and function, the mechanisms underlying this modulation are still elusive. In particular, little is known about the expression and function of nAChRs expressed by individual populations of striatal neurons. In the present study, we used FISH simultaneously probing all major markers of striatal neurons to evaluate expression of beta2-containing nAChRs in the striatum. We also deleted beta2 nicotinic subunit in striatal INs to reveal a functional significance of the relatively scarce population of receptors. Finally, our analysis of c-Fos expression indicated that the beta2-containing nAChRs expressed by striatal INs have overall inhibitory effect on other striatal neurons, both MSNs and INs.

Expression of beta2 nAChR by striatal neurons

Our FISH analysis showed that *Chrn2* mRNA is not particularly abundant in the striatum; and it is present almost exclusively in INs, specifically in CINs, parvalbumin⁺, and NPY⁺ INs. The current knowledge on the expression of

←
del) = 8. An average of 23 VACHT⁺ neurons were analyzed in 4 brain sections per mouse. The 95% credible interval for the odds ratio between ctrl and *beta2-del* [0.09; 1.02], generalized linear mixed model. Data are mean ± SEM. **d**, Representative images showing amphetamine-induced c-Fos expression in control and *beta2-del* animals in combination with VACHT and GFP staining (indicating the AAV-expressing area with presumed beta2 deletion). Left, Two main panels represent merged images for the three markers c-Fos (magenta), GFP (green), and VACHT (gray). Right, Different combinations of two markers are shown, c-Fos/VACHT, GFP/VACHT, and c-Fos/GFP. Yellow arrowheads indicate two VACHT⁺/c-Fos⁻ CINs in *beta2-del* animal.

nAChRs by individual types of striatal neurons primarily arises from electrophysiological studies that detect changes in neuronal firing after the application of nicotine or nAChRs antagonists coupled with optogenetic activation of striatal CINs (Koós and Tepper, 2002; Sullivan et al., 2008; English et al., 2011; Luo et al., 2013; Faust et al., 2015, 2016; Ibáñez-Sandoval et al., 2015; Assous et al., 2017). Most of these studies found the expression of nAChRs in striatal GABAergic neurons (Sullivan et al., 2008; English et al., 2011; Faust et al., 2015, 2016). The FISH data presented here broaden this view: first, they confirm that beta2-containing nAChRs are primarily expressed by striatal INs and not by the MSNs; second, they show that a majority of *Chrn2* mRNA is expressed by CINs in adult mouse striatum. While certain level of *Chrn2* expression by CINs has been previously suggested (Lim et al., 2014; Assous, 2021), CINs have been rarely viewed as the main site of *Chrn2* expression among individual populations of striatal INs. It should be noted that the literature on nicotinic expression by striatal neurons has been quite diverse and sometimes contradictory. In particular, there are data that are both in favor of (Koós and Tepper, 2002) and against (English et al., 2011) the expression of nAChRs by fast-spiking INs. Some discrepancies can also be found in the case of MSNs where at least one study confirms the presence of nAChRs on MSNs (Liu et al., 2007) while others do not (Matsubayashi et al., 2001; Luo et al., 2013). Several factors may contribute to these discrepancies. First, mRNA expression does not necessarily reflect expression on the protein level. Second, in all neuronal populations presented in Muñoz-Manchado et al. (2018), there was a large proportion of cells displaying no expression. This overall low expression may contribute to the contradictory data in literature on nAChR expression by striatal neurons. Last, it has been suggested that the expression of nAChRs in the striatum is strongly age- and learning-dependent (Havekes et al., 2011). In our experiments, we used 3- to 4-month-old mice, while in electrophysiological studies the age of animals is usually lower. Thus, we speculate that the nAChR expression in individual striatal neuronal types flexibly changes during lifetime and is controlled by behavioral state and other mechanisms beyond just the neuron's identity.

Behavioral significance of beta2-containing nAChRs

The DS is involved in the control of multiple behavioral domains. In order to investigate which of them are influenced by beta2-containing nAChRs expressed by striatal INs, we performed numerous behavioral tests. The behavioral phenotype observed in *beta2-del* mice is generally in agreement with previous studies reporting that centrally expressed nAChRs control explorative and social behavior, anxiety-like behavior, and higher cognitive functions (Avale et al., 2011; Picciotto et al., 2015; Koukouli and Changeux, 2020). However, the global KO of beta2 nicotinic subunit has been reported to increase social approach in the social preference test (Avale et al., 2011; Guillem et al., 2011), and higher activity of $\alpha4\beta2$ nAChRs leads to increased anxiety-like behavior in mice (Labarca et al., 2001). During the social preference task, our *beta2-del* mice spent less time in the social compartment compared with controls, but the time spent directly interacting with the social stimulus was not decreased. Instead, the time spent interacting with the non-social object was significantly higher, resulting in a lower sociability ratio. The apparent social deficit in *beta2-del* mice may therefore be more related to impaired exploratory behavior and an altered response to novelty that was also previously reported in *beta2-KO* mice (Granon et al., 2003; Maubourguet et al., 2008). In line

with this, *beta2-del* mice also showed hyperactivity in a novel environment. However, we found a discrepancy between the open field test that did not reveal hyperactivity in *beta2-del* mice and the amphetamine test where the *beta2-del* were clearly hyperactive during the pre-injection habituation period. This can be caused by several factors: the two tasks were performed at different ages as we tested our mice between 3 and 8 months of age; and the open field and amphetamine test were the first and the last task performed, respectively. In relation to this, the beta2 deletion was induced 1 month before the open field testing, while it was in place for 6 months already in case of the amphetamine test. During that period, additional compensatory changes could develop to contribute to hyperactivity in the older *beta2-del* mice. It should be also noted that the broad age span during which the behavioral testing took place could have influenced other behavioral domains as well.

In addition to changes in explorative behavior and locomotion, there was evidence of increased anxiety-like behavior in both the open field and light/dark transition tasks. While changes in this behavior have not been commonly reported in genetic mouse models with beta2-containing nAChR alterations, nicotine and nicotinic agonists and antagonists have been implicated in the control of anxiety and anxiety-like behaviors (Salín-Pascual and Basañez-Villa, 2003; Mineur et al., 2007, 2013; Picciotto et al., 2015). Finally, in *beta2-del* mice, we found an impairment of discrimination learning in the acquisition phase of the response-based T-maze task. This was rather unexpected as striatal ACh has not been previously shown to play a role in the acquisition of discrimination learning (Okada et al., 2018); and instead, its role in cognitive flexibility is well recognized (Prado et al., 2017). However, we were not able to detect any cognitive flexibility impairment in *beta2-del* mice, although we used several different tasks to reveal it. It is conceivable that the impairment of discrimination learning detected in the present study reflects an impaired function of striatal GABAergic neurons expressing nAChRs, as recent studies showed the involvement of striatal SST⁺ and fast spiking (putative PV⁺) GABAergic neurons in instrumental learning and egocentric navigation in the T-maze (Owen et al., 2018; Holly et al., 2019).

In summary, it is quite remarkable that the selective deletion of relatively scarce population of receptors was able to induce a specific behavioral phenotype and that these receptors play a significant role in the control of striatal signaling. It should be noted here that the presented data apply only to male mice that were used exclusively throughout the study. However, a small cohort of female mice that we used in some pilot experiments suggested that the behavioral phenotype induced by beta2 deletion in females may be rather different and the topic requires further investigation.

Activating effect of beta2 deletion on striatal neurons

Through the analysis of c-Fos expression in the striatum, we show that the deletion of beta2-containing nAChRs has an overall activating effect on striatal neurons. This is seemingly in accordance with electrophysiological data suggesting that nicotinic activation of striatal GABAergic neurons leads to inhibition of MSNs (Faust et al., 2016). However, the data indicate that the effect of beta2 deletion in our experiments is more complicated. First, a majority of beta2-containing nAChRs is expressed by CINs themselves; and as CINs realize a very complex control over striatal signaling, it is currently impossible to conclusively predict the effect of this deletion. Second, as shown by our IF analysis, almost 10% of the activated c-Fos-expressing neurons are

DARPP-32-negative cells, presumably INs or possibly astrocytes (Groves et al., 2018). Because neither amphetamine nor beta2-deletion had any effect on the proportion of DARPP-32-negative cells, the idea that it is mostly MSNs that are disinhibited by the beta2 deletion seems unlikely. Rather, the activating effect of the deletion on locomotion and sensitivity to stimulant agrees with the general notion that CINs have overall inhibitory effect, opposing the striatal activation by dopamine. This view is further supported by our data showing that, in contrast to the overall increase in c-Fos induced by beta2 deletion, CINs show rather a decrease of c-Fos expression.

In conclusion, our results show that nAChRs expressed by striatal CINs and other INs inhibit striatal activity. Through this inhibition, they modulate behaviors, including social and exploratory behavior, anxiety-like behavior, and learning. Future studies should determine a possible effect of age and learning on nAChR striatal expression and function.

References

- Angoa-Pérez M, Kane MJ, Briggs DI, Francescutti DM, Kuhn DM (2013) Marble burying and nestlet shredding as tests of repetitive, compulsive-like behaviors in mice. *J Vis Exp*. Advance online publication. Retrieved Dec 24, 2013. doi: 10.3791/50978.
- Assous M (2021) Striatal cholinergic transmission: focus on nicotinic receptors' influence in striatal circuits. *Eur J Neurosci* 53:2421–2442.
- Assous M, Faust TW, Assini R, Shah F, Sidibe Y, Tepper JM (2018) Identification and characterization of a novel spontaneously active bursty GABAergic interneuron in the mouse striatum. *J Neurosci* 38:5688–5699.
- Assous M, Kaminer J, Shah F, Garg A, Koos T, Tepper JM (2017) Differential processing of thalamic information via distinct striatal interneuron circuits. *Nat Commun* 8:15860.
- Avale ME, Chabout J, Pons S, Serreau P, De Chaumont F, Olivo-Marin JC, Bourgeois JP, Maskos U, Changeux JP, Granon S (2011) Prefrontal nicotinic receptors control novel social interaction between mice. *FASEB J* 25:2145–2155.
- Bolte S, Cordelieres FP (2006) A guided tour into subcellular colocalization analysis in light microscopy. *J Microsc* 224:213–232.
- Burbridge TJ, Xu HP, Ackman JB, Ge X, Zhang Y, Ye MJ, Zhou ZJ, Xu J, Contractor A, Crair MC (2014) Visual circuit development requires patterned activity mediated by retinal acetylcholine receptors. *Neuron* 84:1049–1064.
- Bürkner PC (2017) brms: an R package for Bayesian multilevel models using Stan. *J Stat Softw* 80:1–28.
- Cachope R, Mateo Y, Mathur BN, Irving J, Wang HL, Morales M, Lovinger DM, Cheer JF (2012) Selective activation of cholinergic interneurons enhances accumbal phasic dopamine release: setting the tone for reward processing. *Cell Rep* 2:33–41.
- Crawley J, Goodwin FK (1980) Preliminary report of a simple animal behavior model for the anxiolytic effects of benzodiazepines. *Pharmacol Biochem Behav* 13:167–170.
- Deacon RM (2006) Assessing nest building in mice. *Nat Protoc* 1:1117–1119.
- Deacon RM, Rawlins JNP (2006) T-maze alternation in the rodent. *Nat Protoc* 1:7–12.
- Dezfuli G, Olson TT, Martin LM, Keum Y, Siegars BA, Desai A, Uitz M, Sahibzada N, Gillis RA, Kellar KJ (2020) $\alpha 4\beta 2$ nicotinic acetylcholine receptors intrinsically influence body weight in mice. *Neuropharmacology* 166:107921.
- Dumas S, Wallén-Mackenzie Å (2019) Developmental co-expression of Vglut2 and Nurr1 in a mes-di-encephalic continuum precedes dopamine and glutamate neuron specification. *Front Cell Dev Biol* 7:307.
- English DF, Ibanez-Sandoval O, Stark E, Tecuapetla F, Buzsáki G, Deisseroth K, Tepper JM, Koos T (2011) GABAergic circuits mediate the reinforcement-related signals of striatal cholinergic interneurons. *Nat Neurosci* 15:123–130.
- Eskow Jaunarajs KL, Bonsi P, Chesselet MF, Standaert DG, Pisani A (2015) Striatal cholinergic dysfunction as a unifying theme in the pathophysiology of dystonia. *Prog Neurobiol* 127:91–107.
- Faust TW, Assous M, Shah F, Tepper JM, Koós T (2015) Novel fast adapting interneurons mediate cholinergic-induced fast GABAA inhibitory postsynaptic currents in striatal spiny neurons. *Eur J Neurosci* 42:1764–1774.
- Faust TW, Assous M, Tepper JM, Koos T (2016) Neostriatal GABAergic interneurons mediate cholinergic inhibition of spiny projection neurons. *J Neurosci* 36:9505–9511.
- Favier M, Janickova H, Justo D, Kljakic O, Runtz L, Natsheh JY, Pascoal TA, Germann J, Gallino D, Kang JI, Meng XQ, Antinora C, Raulic S, Jacobsen JP, Moquin L, Vigneault E, Gratton A, Caron MG, Duriez P, Brandon MP, et al. (2020) Cholinergic dysfunction in the dorsal striatum promotes habit formation and maladaptive eating. *J Clin Invest* 130:6616–6630.
- Frahm S, Slimak MA, Ferrarese L, Santos-Torres J, Antolin-Fontes B, Auer S, Filkin S, Pons S, Fontaine JF, Tsetlin V, Maskos U, Ibañez-Tallon I (2011) Aversion to nicotine is regulated by the balanced activity of $\beta 4$ and $\alpha 5$ nicotinic receptor subunits in the medial habenula. *Neuron* 70:522–535.
- Franklin KB, Paxinos G (2008) The mouse brain in stereotaxic coordinates. Amsterdam: Elsevier.
- Granon S, Faure P, Changeux JP (2003) Executive and social behaviors under nicotinic receptor regulation. *Proc Natl Acad Sci USA* 100:9596–9601.
- Gras C, Amilhon B, Lepicard EM, Poirer O, Vinatier J, Herbin M, Dumas S, Tzavara ET, Wade MR, Nomikos GG, Hanoun N, Saurini F, Kemel ML, Gasnier B, Giros B, El Mestikawy S (2008) The vesicular glutamate transporter {VGLUT}3 synergizes striatal acetylcholine tone. *Nat Neurosci* 11:292–300.
- Groves A, Kihara Y, Jonnalagadda D, Rivera R, Kennedy G, Mayford M, Chun J (2018) A functionally defined in vivo astrocyte population identified by c-Fos activation in a mouse model of multiple sclerosis modulated by SIP signaling: immediate-early astrocytes (ieAstrocytes). *eNeuro* 5:ENEURO.0239-18.2018.
- Guillem K, Bloem B, Poorthuis RB, Loos M, Smit AB, Maskos U, Spijker S, Mansvelter HD (2011) Nicotinic acetylcholine receptor $\beta 2$ subunits in the medial prefrontal cortex control attention. *Science* 333:888–891.
- Havekes R, Abel T, Van der Zee EA (2011) The cholinergic system and neostriatal memory functions. *Behav Brain Res* 221:412–423.
- Holly EN, Davatolhagh MF, Choi K, Alabi OO, Vargas Cifuentes L, Fuccillo MV (2019) Striatal low-threshold spiking interneurons regulate goal-directed learning. *Neuron* 103:92–101.e6.
- Ibañez-Sandoval O, Xenias HS, Tepper JM, Koós T (2015) Dopaminergic and cholinergic modulation of striatal tyrosine hydroxylase interneurons. *Neuropharmacology* 95:468–476.
- Kamentsky L, Jones TR, Fraser A, Bray MA, Logan DJ, Madden KL, Ljosa V, Rueden C, Eliceiri KW, Carpenter AE (2011) Improved structure, function and compatibility for CellProfiler: modular high-throughput image analysis software. *Bioinformatics* 27:1179–1180.
- Konsolaki E, Tsakanikas P, Polissidis AV, Stamatakis A, Skalioti I (2016) Early signs of pathological cognitive aging in mice lacking high-affinity nicotinic receptors. *Front Aging Neurosci* 8:91.
- Koós T, Tepper JM (2002) Dual cholinergic control of fast-spiking interneurons in the neostriatum. *J Neurosci* 22:529–535.
- Koukoulis F, Changeux JP (2020) Do nicotinic receptors modulate high-order cognitive processing? *Trends Neurosci* 43:550–564.
- Labarca C, Schwarz J, Deshpande P, Schwarz S, Nowak MW, Fonck C, Nashmi R, Kofuji P, Dang H, Shi W, Fidan M, Khakh BS, Chen Z, Bowers BJ, Boulter J, Wehner JM, Lester HA (2001) Point mutant mice with hypersensitive alpha 4 nicotinic receptors show dopaminergic deficits and increased anxiety. *Proc Natl Acad Sci USA* 98:2786–2791.
- Le Moine C, Tison F, Bloch B (1990) D2 dopamine receptor gene expression by cholinergic neurons in the rat striatum. *Neurosci Lett* 117:248–252.
- Lee K, Holley SM, Shobe JL, Chong NC, Cepeda C, Levine MS, Masmanidis SC (2017) Parvalbumin interneurons modulate striatal output and enhance performance during associative learning. *Neuron* 93:1451–1463.e4.
- Legland D, Arganda-Carreras I, Andrey P (2016) MorphoLibJ: integrated library and plugins for mathematical morphology with ImageJ. *Bioinformatics* 32:btw413.
- Léna C, Popa D, Grailhe R, Escourrou P, Changeux JP, Adrien J (2004) Beta2-containing nicotinic receptors contribute to the organization of sleep and regulate putative micro-arousals in mice. *J Neurosci* 24:5711–5718.

- Lim SA, Kang UJ, McGehee DS (2014) Striatal cholinergic interneuron regulation and circuit effects. *Front Synaptic Neurosci* 6:22.
- Liu Z, Otsu Y, Vasuta C, Nawa H, Murphy TH (2007) Action-potential-independent GABAergic tone mediated by nicotinic stimulation of immature striatal miniature synaptic transmission. *J Neurophysiol* 98:581–593.
- Love MI, Huber W, Anders S (2014) Moderated estimation of fold change and dispersion for RNA-seq data with DESeq2. *Genome Biol* 15:550.
- Luo R, Janssen MJ, Partridge JG, Vicini S (2013) Direct and GABA-mediated indirect effects of nicotinic ACh receptor agonists on striatal neurones. *J Physiol* 591:203–217.
- Martos YV, Braz BY, Beccaria JP, Murer MG, Belforte JE (2017) Compulsive social behavior emerges after selective ablation of striatal cholinergic interneurons. *J Neurosci* 37:2849–2858.
- Martyn AC, De Jaeger X, Magalhães AC, Kesarwani R, Gonçalves DF, Raulic S, Guzman MS, Jackson MF, Izquierdo I, Macdonald JF, Prado MA, Prado VF (2012) Elimination of the vesicular acetylcholine transporter in the forebrain causes hyperactivity and deficits in spatial memory and long-term potentiation. *Proc Natl Acad Sci USA* 109:17651–17656.
- Matsubayashi H, Amano T, Amano H, Sasa M (2001) Excitation of rat striatal large neurons by dopamine and/or glutamate released from nerve terminals via presynaptic nicotinic receptor (A4beta2 type) stimulation. *Jpn J Pharmacol* 86:429–436.
- Maubourguet N, Lesne A, Changeux JP, Maskos U, Faure P (2008) Behavioral sequence analysis reveals a novel role for beta2* nicotinic receptors in exploration. *PLoS Comput Biol* 4:e1000229.
- Mineur YS, Somenzi O, Picciotto MR (2007) Cytisine, a partial agonist of high-affinity nicotinic acetylcholine receptors, has antidepressant-like properties in male C57BL/6J mice. *Neuropharmacology* 52:1256–1262.
- Mineur YS, Obayemi A, Wigstrand MB, Fote GM, Calarco CA, Li AM, Picciotto MR (2013) Cholinergic signaling in the hippocampus regulates social stress resilience and anxiety- and depression-like behavior. *Proc Natl Acad Sci USA* 110:3573–3578.
- Muñoz-Manchado AB, Foldi C, Szydłowski S, Sjulson L, Farries M, Wilson C, Silberberg G, Hjerling-Leffler J (2016) Novel striatal GABAergic interneuron populations labeled in the 5HT3a(EGFP) mouse. *Cereb Cortex* 26:96–105.
- Muñoz-Manchado AB, Bengtsson Gonzales C, Zeisel A, Munguba H, Bekkouche B, Skene NG, Lonnerberg P, Ryge J, Harris KD, Linnarsson S, Hjerling-Leffler J (2018) Diversity of interneurons in the dorsal striatum revealed by single-cell RNA sequencing and Patchseq. *Cell Rep* 24:2179–2190.e7.
- Nadler JJ, Moy SS, Dold G, Simmons N, Perez A, Young NB, Barbaro RP, Piven J, Magnuson TR, Crawley JN, Crawley JN (2004) Automated apparatus for quantitation of social approach behaviors in mice. *Genes Brain Behav* 3:303–314.
- Okada K, Nishizawa K, Setogawa S, Hashimoto K, Kobayashi K (2018) Task-dependent function of striatal cholinergic interneurons in behavioural flexibility. *Eur J Neurosci* 47:1174–1183.
- Ollion J, Cochenec J, Loll F, Escudé C, Boudier T (2013) TANGO: a generic tool for high-throughput 3D image analysis for studying nuclear organization. *Bioinformatics* 29:1840–1841.
- Owen SF, Berke JD, Kreitzer AC (2018) Fast-spiking interneurons supply feedforward control of bursting, calcium, and plasticity for efficient learning. *Cell* 172:683–695.e15.
- Picciotto M, Caldarone BJ, King SL, Zachariou V (2000) Nicotinic receptors in the brain links between molecular biology and behavior. *Neuropsychopharmacology* 22:451–465.
- Picciotto MR, Lewis AS, van Schalkwyk GI, Mineur YS (2015) Mood and anxiety regulation by nicotinic acetylcholine receptors: a potential pathway to modulate aggression and related behavioral states. *Neuropharmacology* 96:235–243.
- Polidarová L, Sládek M, Nováková M, Parkanová D, Sumová A (2013) Increased sensitivity of the circadian system to temporal changes in the feeding regime of spontaneously hypertensive rats: a potential role for Bmal2 in the liver. *PLoS One* 8:e75690.
- Prado VF, Janickova H, Al-Onaizi MA, Prado MA (2017) Cholinergic circuits in cognitive flexibility. *Neuroscience* 345:130–141.
- Quik M, Wonnacott S (2011) $\alpha 6\beta 2^*$ and $\alpha 4\beta 2^*$ nicotinic acetylcholine receptors as drug targets for Parkinson's disease. *Pharmacol Rev* 63:938–966.
- Quik M, Huang LZ, Parameswaran N, Bordia T, Campos C, Perez XA (2009) Multiple roles for nicotine in Parkinson's disease. *Biochem Pharmacol* 78:677–685.
- Rapanelli M, Frick LR, Xu M, Groman SM, Jindachomthong K, Tamamaki N, Tanahira C, Taylor JR, Pittenger C (2017) Targeted interneuron depletion in the dorsal striatum produces autism-like behavioral abnormalities in male but not female mice. *Biol Psychiatry* 82:194–203.
- Rodriguez A, Zhang H, Klaminder J, Brodin T, Andersson PL, Andersson M (2018) ToxTrac: a fast and robust software for tracking organisms. *Methods Ecol Evol* 9:460–464.
- Rossato JJ, Bevilacqua LR, Medina JH, Izquierdo I, Cammarota M (2006) Retrieval induces hippocampal-dependent reconsolidation of spatial memory. *Learn Mem* 13:431–440.
- Salín-Pascual RJ, Basañez-Villa E (2003) Changes in compulsion and anxiety symptoms with nicotine transdermal patches in non-smoking obsessive-compulsive disorder patients. *Rev Invest Clin* 55:650–654.
- Schindelin J, Arganda-Carreras I, Frise E, Kaynig V, Longair M, Pietzsch T, Preibisch S, Rueden C, Saalfeld S, Schmid B, Tinevez JY, White DJ, Hartenstein V, Eliceiri K, Tomancak P, Cardona A (2012) Fiji: an open-source platform for biological-image analysis. *Nat Methods* 9:676–682.
- Schmidt U, Weigert M, Broaddus C, Myers G (2018) Cell detection with star-convex polygons. *arXiv:1806.03535*.
- Sullivan MA, Chen H, Morikawa H (2008) Recurrent inhibitory network among striatal cholinergic interneurons. *J Neurosci* 28:8682–8690.
- Threlfell S, Lalic T, Platt NJ, Jennings KA, Deisseroth K, Cragg SJ (2012) Striatal dopamine release is triggered by synchronized activity in cholinergic interneurons. *Neuron* 75:58–64.
- Venables WN, William N, Ripley BD (1994) *Modern applied statistics with S*. New York:Springer-Verlag New York Inc.
- Walf AA, Frye CA (2007) The use of the elevated plus maze as an assay of anxiety-related behavior in rodents. *Nat Protoc* 2:322–328.
- Wang X, Bey AL, Katz BM, Badea A, Kim N, David LK, Duffney LJ, Kumar S, Magee SD, Hulbert SW, Dutta N, Hayrapetyan V, Yu C, Gaidis E, Zhao S, Ding JD, Xu Q, Chung L, Rodriguiz RM, Wang F, et al. (2016) Altered mGluR5-Homer scaffolds and corticostriatal connectivity in a Shank3 complete knockout model of autism. *Nat Commun* 7:11459.
- Wickham H (2016) *ggplot2: elegant graphics for data analysis*. New York: Springer.
- Yates JW, Meij JT, Sullivan JR, Richtand NM, Yu L (2007) Bimodal effect of amphetamine on motor behaviors in C57BL/6 mice. *Neurosci Lett* 427:66–70.
- Zhang R, Xue G, Wang S, Zhang L, Shi C, Xie X (2012) Novel object recognition as a facile behavior test for evaluating drug effects in A β PP/PS1 Alzheimer's disease mouse model. *J Alzheimers Dis* 31:801–812.